




Osteosarcoma cell death induced by innovative scaffolds doped with chemotherapeutics

Carmen Lanzillotti¹ | Maria Rosa Iaquina¹ | Raffaella De Pace¹ |
 Maria Mosaico¹ | Simone Patergnani² | Carlotta Giorgi² | Marta Tavoni³ |
 Massimiliano Dapporto³ | Simone Sprio³ | Anna Tampieri³ | Monica Montesi³  |
 Fernanda Martini^{1,4}  | Elisa Mazzoni⁵ 

¹Laboratories of Cell Biology and Molecular Genetics, Department of Medical Sciences, University of Ferrara, Ferrara, Italy

²Laboratories of Cell Signalling, Department of Medical Sciences, University of Ferrara, Ferrara, Italy

³Institute of Science, Technology and Sustainability for Ceramics, National Research Council of Italy (ISSMC-CNR, former ISTECC-CNR), Faenza, Italy

⁴Laboratory for Technologies of Advanced Therapies (LTTA), University of Ferrara, Ferrara, Italy

⁵Department of Chemical, Pharmaceutical and Agricultural Sciences, University of Ferrara, Ferrara, Italy

Correspondence

Elisa Mazzoni, Department of Chemical, Pharmaceutical and Agricultural Sciences, University of Ferrara, Ferrara, Italy.
 Email: elisa.mazzoni@unife.it

Monica Montesi, Institute of Science, Technology and Sustainability for Ceramics, National Research Council of Italy (ISSMC-CNR, former ISTECC-CNR), Faenza, Italy.
 Email: monica.montesi@issmc.cnr.it

Fernanda Martini, Laboratories of Cell Biology and Molecular Genetics, Department of Medical Sciences, University of Ferrara, Ferrara, Italy.
 Email: mrf@unife.it

Funding information

POR FSE, European Union; Ministero della Università e della Ricerca (MUR) PRIN 2017;

Abstract

Osteosarcoma (OS) cancer treatments include systemic chemotherapy and surgical resection. In the last years, novel treatment approaches have been proposed, which employ a drug-delivery system to prevent offside effects and improves treatment efficacy. Locally delivering anticancer compounds improves on high local concentrations with more efficient tumour-killing effect, reduced drugs resistance and confined systemic effects. Here, the synthesis of injectable strontium-doped calcium phosphate (SrCPC) scaffold was proposed as drug delivery system to combine bone tissue regeneration and anticancer treatment by controlled release of methotrexate (MTX) and doxorubicin (DOX), coded as SrCPC-MTX and SrCPC-DOX, respectively. The drug-loaded cements were tested in an in vitro model of human OS cell line SAOS-2, engineered OS cell line (SAOS-2-eGFP) and U2-OS. The ability of doped scaffolds to induce OS cell death and apoptosis was assessed analysing cell proliferation and Caspase-3/7 activities, respectively. To determine if OS cells grown on doped-scaffolds change their migratory ability and invasiveness, a wound-healing assay was performed. In addition, the osteogenic potential of SrCPC material was evaluated using human adipose derived-mesenchymal stem cells. Osteogenic markers such as (i) the mineral matrix deposition was analysed by alizarin red staining; (ii) the osteocalcin (OCN) protein expression was investigated by enzyme-linked immunosorbent assay test, and (iii) the osteogenic process was studied by real-time polymerase chain reaction array. The delivery system induced cell-killing cytotoxic effects and apoptosis in OS cell lines up to Day 7. SrCPC demonstrates a good cytocompatibility and it induced upregulation of osteogenic genes involved in the skeletal development pathway, together with OCN protein expression and mineral matrix deposition. The proposed approach, based on the local, sustained release of anticancer drugs from nanostructured biomimetic drug-loaded cements is

Carmen Lanzillotti and Maria R. Iaquina contributed equally to the work.

This is an open access article under the terms of the [Creative Commons Attribution-NonCommercial-NoDerivs](https://creativecommons.org/licenses/by-nc-nd/4.0/) License, which permits use and distribution in any medium, provided the original work is properly cited, the use is non-commercial and no modifications or adaptations are made.

© 2024 The Authors. *Journal of Cellular Physiology* published by Wiley Periodicals LLC.

University of Ferrara, Fondo di Ateneo per la Ricerca, Grant/Award Number: FAR 2021

promising for future therapies aiming to combine bone regeneration and anticancer local therapy.

KEYWORDS

apoptosis, calcium phosphate bone cement, drug delivery, mesenchymal stem cell, osteosarcoma

1 | INTRODUCTION

Osteosarcoma (OS) is the most common malignant bone cancer, which mainly affects children and adolescents (Belayneh et al., 2021; Jackson et al., 2016). OS represents the cause of 8.9% of cancer-related deaths (Ottaviani & Jaffe, 2009). Moreover, OS is 1.4 times more frequent in males than in females (Ritter & Bielack, 2010) and in Afro-Americans and Hispanics than Caucasians (Ottaviani & Jaffe, 2009). It is the most common primary skeletal tumour of childhood and adolescence, with a yearly incidence of 5.6 cases per million in children under the age of 15 (Belayneh et al., 2021; Jackson et al., 2016). OS rarely occurs in children younger than 5 years old and, in this case, is associated with a cancer susceptibility syndrome, known as Li-Fraumeni syndrome (Jackson et al., 2016). OS has a bimodal age distribution, with the first peak in children and young adults occurring in patients 10–30 years old and a second peak in the elderly patients 70–80 years old (Mirabello et al., 2009). The first peak corresponds to the pubertal growth spurt suggesting a relationship between OS occurrence and bone cell proliferation (Ritter & Bielack, 2010). The second OS peak is represented by secondary bone lesions, often related to Paget's disease, different radio-therapies or a genetic predisposition to syndromes, including retinoblastoma 1 (Jackson et al., 2016; Kumar et al., 2018). Recent investigations support the hypothesis that OS originates from mesenchymal stem/stromal cells (MSCs) and/or in more committed osteoblastic precursors (Gaebler et al., 2017; Mutsaers & Walkley, 2014).

OS treatments include systemic chemotherapy and surgical resection (Jafari et al., 2020). Surgery on growing young patients with an immature skeleton can create significant limb-length discrepancy and gait abnormalities (Lewis, 2005). Surgery is the primary OS treatment, consisting in the tumour mass removal. However, often the entire limbs are removed (Beaury et al., 2018). Therefore, after the tumour mass resection the major problems are: (i) the regeneration of bone structure to address aesthetic and functional activities and (ii) the prevention of cancer relapses (Bischoff et al., 2018). The survival rate is increased by the progress of destructive systemic chemotherapies. The most commonly employed chemotherapeutic agents are high-dose methotrexate (MTX) and doxorubicin (DOX) (Beaury et al., 2018; Xu et al., 2014). Since the introduction of chemotherapies to treat OS in late 70s, patients diagnosed with OS receive a neo-adjuvant treatment followed by a post-surgery adjuvant therapy with a cocktail of chemotherapies, that is, high-dose MTX (12 g/m²), etoposide and ifosfamide for children and young adults (<25 years) or other

protocols, combining DOX, cisplatin and ifosfamide with or without high-dose MTX (Bishop et al., 2016). Leucovorin, widely co-administered to reduce the toxic effects of MTX, is still a harmful therapy to patients (Xu et al., 2014). The choice and use of chemotherapeutic drugs against OS is still controversial. OS treatments may present complications due to toxicity of chemotherapeutic agents, such as alopecia, myelosuppression, mucositis, nausea, and vomiting, as well as late effects including cardiac toxicity, acute and chronic nephrotoxicity, neurotoxicity, hearing loss, infertility and second malignant neoplasms (Janeway & Grier, 2010). In addition, a serious drawback is related to nonspecific killing effects against cancer and healthy cells elicited by drugs used in chemotherapy (Bischoff et al., 2018; Harrison & Schwartz, 2017). Reported therapeutic regimens, the 5-year survival has reached 78% for children and young adults with localized bone cancer, but still remains at only 20% in patients with metastasis at diagnosis or in relapse (Corre et al., 2020).

In the last years, novel treatment approaches have been proposed, which employ a drug-delivery system to prevent offside effects and improves treatment efficacy. Indeed, locally delivering anticancer compounds improves on high local concentrations with more efficient tumour-killing effect, reduced drugs resistance and confined systemic effects (Jafari et al., 2020; Liao et al., 2021). Together with the treatment of cancer cells avoiding side effect for the patient, there is another important clinical need to take into consideration in the cancer therapy approach, such as the regeneration of new healthy bone after eradication of diseased tissue.

Hence, the development of bioactive bone substitutes combining effective regenerative and antitumor features over time is highly demanded. Bone regrowth, as well as regenerative medicine in general, has emerged as a multidisciplinary field, which takes advantage of knowledge in different sciences, such as materials science, cell biology, tissue engineering, molecular genetics, and epigenetics (Iaquinta et al., 2019; Oton-Gonzalez et al., 2022). Bone tissue in physiological conditions has the ability to regenerate itself, while bone fractures due to bone cancer may have compromised healing capacity (Ho-Shui-Ling et al., 2018). Several studies in tissue engineering, combined with regenerative medicine (Mazzoni et al., 2021b), have previously attempted to develop scaffolds, similar to bone structure and composition with cytocompatibility and osteoinductivity properties to induce cell proliferation and osteogenic differentiation in the affected sites (Mazzoni et al., 2021a; Mazzoni et al., 2023). In previous investigations we employed, as an in vitro cellular model, primary human adipose derived-MSCs (hASCs) to

analyse the cytocompatibility and osteoinductivity properties of biomaterials (laquinta et al., 2021b; laquinta et al., 2022; Mazzoni et al., 2017; Sprio et al., 2020).

Moreover, other studies also demonstrated that various materials could be employed as drug delivery systems for anticancer therapies (Sobczak & Kędra, 2022; Son & Kim, 2017; Tanzawa et al., 2011; Wu et al., 2020). It has been reported that Hydroxyapatite (HA)-cyclodextrin-DOX chemotherapeutic strategy, for example, may enhance the drug-targeting effect on tumour cells while protecting the more sensitive healthy cells for a period of time after implantation (Bischoff et al., 2018). In addition, in the last decades calcium phosphate bone cements (CPCs) have been proposed as a valuable type of scaffold for regenerating bone defects, associated with multiple strategies for effective drug loading and controlled release, especially for the treatment of bone cancer (Pylostomou et al., 2023). In this context, Sr-doped CPCs or bioglasses have attracted increasing interest in recent years (Cui et al., 2020; Liu et al., 2023; Schumacher & Gelinsky, 2015). These biomaterials are prepared by mixing a powder and a liquid, resulting in the formation of a viscous and injectable paste provided with self-hardening capacity, due to the progressive dissolution of the precursor powder and precipitation of more stable calcium phosphates (e.g., HA). Besides, such injectable paste comes with the unique benefit to fill complex-shape bone defects, while also providing therapeutic ions incorporated into the biomaterial. It was demonstrated that a small amount of Sr²⁺ ions doping resulted effective in enhancing stem cell proliferation and modulating osteoblast and osteoclast cells fate in vitro, targeting the re-equilibration of the natural bone turnover in osteoporosis scenario (Montesi et al., 2017).

In this study, strontium-doped apatitic CPCs were prepared to combine the antiosteoporotic ability of strontium (Marie, 2005; Sprio et al., 2016) and the well-established osteointegrative properties of CPCs to sustain the regeneration of bone tissue. The cement was designed as effective carrier for MTX or DOX drugs, clinically used for the treatment of bone cancer patients. Their biological performance was tested in hASCs and human OS cell lines, that is, SAOS-2, SAOS-2-eGFP and U2-OS. The present work aims to combine anticancer effect with the well-assessed regenerative potential of calcium phosphate cements and may represent a valuable approach against OS.

2 | MATERIALS AND METHODS

2.1 | Preparation and characterization of strontium-doped calcium phosphate scaffold (SrCPC) materials

The SrCPCs tested in this work were prepared as previously reported (Sprio et al., 2016). Briefly, Sr-doped α -tricalcium phosphate (α -Sr_xCa_{3-x}(PO₄)₂: Sr- α TCP) powders according to Sr/(Ca+Sr) \approx 2 mol% were synthesized by dry mixing proper amount of calcium carbonate (CaCO₃, Sigma Aldrich), dicalcium phosphate dibasic anhydrous

(CaHPO₄, Sigma Aldrich) and strontium carbonate (SrCO₃, Sigma Aldrich), followed by thermal treatment at 1400°C for 1 h and rapid cooling. Then, the powders were milled by planetary mono mill (Pulverisette 6 classic line, Fritsch) for 50 min at 400 rpm using a zirconia jar with 5 mm diameter grinding media. The liquid component of the paste was made of aqueous solutions of disodium hydrogen phosphate dihydrate, 5 wt% (Na₂HPO₄ · 2H₂O, Fluka) and sodium alginate, 2 wt% (Alginic Acid Sodium Salt from Brown Algae, Sigma Aldrich). The functionalization of the cements was carried out by mixing the drug with cement precursor before mixing with cement liquid phase (e.g., 10 mg of drug were mixed with 3 g of powders) (lafisco et al., 2016; Sarda et al., 2018). The cements were finally prepared according to liquid-to-powder ratio equal to 0.6, by high-energy shear mixing of powder and liquid phases to improve the homogeneity of the final cements, as previously observed (Dapporto et al., 2021). For each sample, disk-shaped specimens (diameter = 10 mm, height = 2 mm, weight \approx 450 mg) were obtained. The drug release kinetics were investigated upon immersion in 2 mL of HEPES 0.01 M at pH 7.4 in KCl 0.01 M, with daily measurement by UV-vis spectrophotometer (LAMBDA™ 750 UV/Vis/NIR spectrophotometer from PerkinElmer) at 306 and 480 nm. The physical mechanisms underlying the drug release were further investigated and hypothesized based on previously reported mathematical models. In particular, the Power Law model ($\chi_t = Kt^n$) was identified as semiempirical model able to describe drug release from polymeric or monolithic systems (Bruschi, 2015; Fosca et al., 2022; Korsmeyer et al., 1983; Paarakh et al., 2019). In this model, χ_t is the fraction of the released drug by time t , K is a parameter including geometrical and structural features of the matrix, and n is as a coefficient related to the mechanism that governs the release kinetic, according to Supporting Information S1: Material S1–S3. Before the cell seeding, scaffolds were sterilized with two washes of ethanol 70% (20 min/each), phosphate-buffered saline (PBS) 1 \times (10 min/each) and ultraviolet (UV) light (60 min/side) and kept in 5 mL of medium at 37°C for 3 days, in sterile conditions.

2.2 | Cell cultures

In this study, the in vitro assays were performed using OS cell lines, that is, U2-OS, SAOS-2, and SAOS-eGFP. SAOS-2 were originally purchased from ATTC, Cat. no. HTB-85 (Morelli et al., 2007). The engineered SAOS-eGFP cells were derived from parental SAOS-2 cells engineered with the enhanced green fluorescent protein (eGFP)-expressing gene (Globig et al., 2020; Manfrini et al., 2015; Morelli et al., 2007). SAOS-eGFP cell line were expanded in Dulbecco's Modified Eagle Medium F-12 (DMEM/F12; Lonza) with 10% fetal bovine serum (FBS) and 1% of Geneticin (Invitrogen) and kept in a humidified atmosphere at 37°C with 5% CO₂ (Manfrini et al., 2015). U2-OS cells were purchased from ATTC, Cat. no. HTB-96, cultured in McCoy's (Lonza) with 10% FBS and 1% of P/S, and kept in a humidified atmosphere at 37°C with 5% CO₂. OS cells were seeded with a concentration of 1.5 \times 10⁴ cells per well and grown on

(i) SrCPC-MTX, (ii) SrCPC-DOX and (iii) drug-free SrCPC, as control, until the time of the analysis (Manfrini et al., 2015).

The compatibility and osteoinductivity of SrCPC scaffolds was evaluated using hASC cultures, at Day 14. The hASCs used in this study were purchased from Lonza, PT-5006, as cryopreserved frozen cells at the first passage. The company certified that hASCs are positive for surface markers CD13, CD29, CD44, CD73, CD90, CD105 and CD166, while being negative for other markers, such as CD14, CD31 and CD45. Cells were expanded in α -MEM (Lonza) supplemented with 20% FBS, antibiotics and maintained in a humidified atmosphere at 37°C with 5% CO₂ (Mazzoni et al., 2020). The hASCs were seeded with a concentration of 1.5×10^4 cells per well and were grown on (i) SrCPC scaffold and (ii) the tissue culture polystyrene (TCPS) vessels, as control, until the analysis.

2.3 | Scanning electron microscopy (SEM) analyses

SEM analysis was carried out to investigate the structure of SrCPC, SrCPC-MTX, and SrCPC-DOX biomaterials and to analyse cell-cement interaction. To this purpose, SAOS and U2-OS cells (1.5×10^4) were grown on SrCPC-MTX, SrCPC-DOX scaffolds and drug-free SrCPC, as control, up to Day 7, whereas hASCs (1.5×10^4) were grown on SrCPC scaffold up to Day 14. After cell culture, scaffolds were washed with PBS 1 \times and fixed for 1 h by 2.5% glutaraldehyde and 4 h by 1% osmium solution in phosphate buffer. Samples were sputter-coated with gold and observed SEM (Cambridge, model Stereoscan S-360) (Mazzoni et al., 2020). The analysis was performed in triplicate for each experimental group.

2.4 | Alamar Blue assay

The metabolic activity of SAOS and U2-OS grown on SrCPC-MTX and SrCPC-DOX scaffolds was evaluated using the Alamar Blue assay (Invitrogen). Cells were incubated in medium with 5% of Alamar Blue reagent for 3 h at 37°C. A concentration of 1.6×10^5 cells and serial 1:2 dilutions were seeded to generate a calibration curve consisting of scalar concentration of SAOS and U2-OS cells up to 5000 cells. In addition, the metabolic activity rate of hASCs grown on the SrCPC scaffold and TCPS, as controls, was determined using the Alamar Blue assay at Day 1, 2 and 7. Supernatant optical density was measured at a 570 nm wavelength and at a 620 nm reference wavelength using a spectrophotometer (Thermo Electron Corporation, model Multiskan EX) (Iaquinta et al., 2022). The analysis was performed in triplicate for each experimental group. Each experimental group was tested at different time points, that is, at Day 1, 2 and 7 (Manfrini et al., 2013).

2.5 | SAOS-eGFP cells fluorescence analysis

Digital images of SAOS-eGFP cells grown on drug-free SrCPC, SrCPC-MTX and SrCPC-DOX scaffolds were obtained using a

confocal microscope (LSM510; Carl Zeiss) with a 10 \times 1.4 NA Plan-Apochromat oil-immersion objective and equipped with ZEN microscope imaging software (Carl Zeiss). The SAOS-eGFP cells fluorescence intensity mean for each sample was evaluated using ImageJ software as previous reported analysis was performed at Day 7.

2.6 | Annexin V/propidium iodide (PI)

The Tali[®] Apoptosis Kit-Annexin V Alexa Fluor[®] 488 and Propidium Iodide (Life Technologies, Cat. no. A10788) was used to determine if cells grown on (i) SrCPC-MTX, (ii) SrCPC-DOX and (iii) drug-free SrCPC employed as control are apoptotic/necrotic at Day 4. Cells grown on scaffolds were trypsinized, washed with 1 \times PBS and centrifuged at 8000g for 10 min. After discarding the supernatant, OS cell lines were incubated with 100 μ L Annexin-binding buffer (1 \times) and 5 μ L of Annexin-V Alexa Fluor[®] 488 per sample, for 20 min. Then, cells were incubated for 3 min at room temperature (RT) in 1 μ L of PI. Finally, cells were loaded into a Tali[®] Cellular Analysis Slide and analysed using the Tali[®] Image-Based Cytometer. Data were collected using the Tali[®] data acquisition and analysis software (Life Technologies).

2.7 | Caspase-3/7 activities

Caspase 3/7 activities were analysed using the CellEvent[™] Caspase-3/7 Green detection reagent (Life Technologies, cat: C10723) according to manufacturer's instructions. Briefly, SAOS-2 and U2-OS cells (1×10^5 cells/well) were seeded in 24-well plate on Sr-CPC, SrCPC-DOX and SrCPC-MTX materials for 4 days. After incubation, cells were labelled with 5 μ M CellEvent[™] Caspase-3/7 green detection reagent in PBS 1 \times and 5% FBS. Stained cells were observed through fluorescence microscope (LSM510; Carl Zeiss) using a 10 \times 1.4 NA Plan-Apochromat oil-immersion objective and equipped with ZEN microscope imaging software (Carl Zeiss). Digital Images were acquired in z-stacks at 8 μ m. All experiments were performed independently in triplicate.

2.8 | Enzyme-linked immunosorbent assay (ELISA) to semiquantified caspase-3

Semiquantification of cleaved caspase-3 protein was detected by using RayBio[®] CASP-3 (D175) ELISA Kit (RayBio[®] cat: PTE-CASP3-D175-T). This sandwich ELISA is for measuring cleaved CASP-3 (Asp-175) as well as caspase-3 in human cell lysates. Briefly, SAOS-2 cells and U2-OS (1×10^5 cells/well) were seeded in 24-well plate on SrCPC, SrCPC-DOX and SrCPC-MTX biomaterials for 4 days. Absorbance of the developed chromophore was measured using a colorimetric ELISA reader (Thermo Electron Corporation, model Multiskan EX) at a wavelength (λ) of 450 nm. Total caspase 3 and activated/cleaved caspase-3 activity were measured as the ratio

between activated and total caspase 3. The data were reported as OD median value and SD. Experiments were performed in technical triplicate for each biological sample ($n = 3$).

2.9 | Wound-healing assay

OS cell lines were seeded on the lower surface of the transwell (Corning, Cat. no. 3450, Merck), whereas the SrCPC, SrCPC-MTX and SrCPC-DOX scaffolds were placed on the upper surface of the transwell insert. OS cell lines were seeded at a density of 1.0×10^5 cells/well and cultured at 37°C with 5% CO₂ until they reached 90% confluence, which was necessary to initiate the assay. Following the creation of the scratch using a 1000 µL pipette tip on the bottom surface of the cell monolayer (two dimension), the effect of SrCPC-MTX and SrCPC-DOX scaffolds on cell migration ability was observed, compared to the control group (SrCPC). Image acquisition occurred at different time points, that is, 24, 48, and 72 h, using a bright-field microscope (TE2000E Nikon Instruments, Sesto Fiorentino). Digital images were acquired using ACT-1 and ACT-2 software for DXM 1200F digital cameras (Nikon Instruments) at $\times 4$ magnification. The experiment was performed in triplicate for each experimental group. Cell migration capacity was measured by comparing the healed area of the scratch among different experimental conditions. The scratch areas were measured and analysed using ImageJ software (National Institutes of Health Bethesda) and results were expressed as the average percentage of wound closure (%) up to 72 h.

2.10 | Live/Dead assay

Cytocompatibility of hASCs grown on scaffolds was assessed by Live/Dead dye and confocal laser scanning microscopy at Day 3, 6 and 14. Live/Dead Cell Double Staining Kit for mammalian cells (Calbiochem) was employed to analyse the viability of hASCs grown on biomaterials. Live/Dead assay was performed according to the manufacturer's instructions. Cell-permeable green fluorescent Cyto-dye (Ex. max.: 488 nm; Em. max.: 518 nm) was used to stain live cells, whereas PI (Ex. max.: 488 nm; Em. max.: 615 nm) was used to stain dead cells. Scaffolds were kept in saline solution during analysis with confocal microscope (LSM510; Carl Zeiss) using a 10×1.4 NA Plan-Apochromat oil-immersion objective and equipped with ZEN microscope imaging software (Carl Zeiss). Digital Images were acquired in z-stacks at 0.5 µm. Moreover, Live/Dead assay was performed in cells grown on glass slide in contact with SrCPC scaffold and on TCPS, as control. Digital images were acquired at TE 200-E fluorescent microscope through ACT-1 software for DXM120F digital cameras (Nikon Instruments) at $\times 20$ magnification and analysed using ImageJ software (National Institutes of Health Bethesda) (Zhu et al., 2013). Experiments were performed in technical triplicate for each biological sample ($n = 3$).

2.11 | Cytoskeleton architecture

hASCs grown on SrCPC scaffolds were assessed by tetramethyl-rhodamine-iso-thio-cyanate (TRITC) conjugated-Phalloidin (Sigma) to stain cytoskeleton filaments, binding F-actin, at Day 14. The cells were washed with PBS 1 \times and fixed with formalin 10% for 10 min at RT. Afterwards, cell nuclei were marked with 0.5 mg/mL 4',6-diamidino-2-phenylindole (DAPI) (Invitrogen). Cell cytoskeleton analysis at $\times 40$ magnification were carried out with Olympus Xcellence multiple wavelength high-resolution fluorescence microscopy system (Olympus) and analysed using ImageJ software (National Institutes of Health Bethesda) (Giorgi et al., 2014).

Moreover, hASC intermediate filaments were studied analysing the immunofluorescence of the vimentin protein. Briefly, hASCs were washed with PBS 1 \times and fixed in methanol/acetone 1:1 for 7 min at -20°C . After PBS 1 \times washing, cells were permeabilized with 0.1% Triton X-100 in PBS 1 \times for 10 min at RT. Cells were incubated with rabbit anti-vimentin (Cat. no. PA5-27231 Thermo Fisher) primary antibody 1:100 in PBS 1 \times containing 3% bovine serum albumin (BSA) for 1 h at 37°C, washed with PBS 1 \times and incubated with Alexa Fluor 488-conjugated secondary antibody (Cat. no. A-21206, Thermo Fisher) at a dilution of 1:200 in PBS 1 \times containing 3% BSA for 1 h at 37°C. Cell nuclei were stained with DAPI (Thermo Fisher) and images were acquired with a TE 200-E fluorescent microscope. Images were obtained through ACT-1 software for DXM120F digital cameras (Nikon Instruments). The analyses were performed in triplicate for each experimental group.

2.12 | Human extracellular matrix (ECM), adhesion molecules and osteogenesis RT² Profiler PCR array

hASCs were grown on tested SrCPC scaffold and TCPS control up to Day 14. At Days 3, 6 and 14, RNA was isolated using the RNeasy Plus Micro Kit (Qiagen) following provided protocol. RNA quality and quantity was evaluated using a Nanodrop spectrophotometer (ND-1000, Nanodrop Technologies, Thermo Fischer Scientific) (Manfrini et al., 2015; Mazzoni et al., 2021a), then reverse-transcribed to complementary DNA (cDNA) using the RT² First Strand cDNA Kit as recommended (Qiagen). The analysis was performed in triplicate for each experimental group. The human ECM and adhesion molecules PCR Array (Qiagen, cat: PAHS-013Z) was employed to analyse the genes modulated in hASCs grown on SrCPC scaffold at Day 3, 6 and 14. The RT² Profiler PCR Array for ECM and adhesion molecules allowed analysing the expression of 84 genes involved in cell-to-cell adhesion, cells to the ECM adhesion and five housekeeping genes. Analyses were carried out using SYBR Green method on a CFX96 Touch™ PCR detection system (Bio-Rad) (Mazzoni et al., 2020). The human Osteogenesis PCR Array (Qiagen, cat: PAHS-026Z), performed in triplicate, was assessed to identify genes, which are involved in osteogenic pathways modulated by SrCPC scaffolds in hASCs at Day 3, 6 and 14. RT² Profiler PCR Array for human

osteogenesis was employed in real-time polymerase chain reaction (PCR) to analyse the expression of 84 genes involved in skeletal development and bone mineral metabolism, as well as cell adhesion molecules. Analyses were carried out using SYBR Green method on a CFX96 Touch™ PCR detection system (Bio-Rad) (Mazzoni et al., 2020).

2.13 | Alizarin red staining assay in hASCs grown on SrCPC scaffold

The mineral matrix deposition, employed as osteogenic marker, was investigated by Alizarin Red staining in hASCs grown on different experimental conditions represented by (i) the SrCPC biomaterial and (ii) TCPS, up to Day 14 in basal culture medium constituted by α MEM (Lonza) supplemented with 20% FBS and antibiotics (Mazzoni et al., 2020). Human ASCs grown on SrCPC scaffold and TCPS, for 14 days, were fixed in 4% neutral buffered formalin and stained with a 40 mM, pH 4.2 solution of Alizarin Red (Sigma-Aldrich) to analyse the mineral matrix deposition. After extensive washing, to remove unbound staining, pictures were taken using a standard light microscope (Nikon Eclipse TE 2000-E microscope, Nikon Instruments Spa) equipped with a digital camera (DXM 1200F; Nikon Instruments Spa). Afterwards, the mineralized substrates were dissolved using 20% methanol and 10% acetic acid in a water solution (Sigma-Aldrich), whereas the quantification was carried out, in triplicate, using a spectrophotometer (Thermo Electron Corp., model Multiskan EX) at a wavelength (λ) of 450 nm. The analysis was performed in triplicate for each experimental group.

2.14 | Osteocalcin (OCN) protein expression

The ELISA test was carried out at Day 14 to identify OCN protein expression in hASCs grown on SrCPC scaffold and on TCPS (control group). Protein extraction was performed using Cell Extraction Buffer (Thermo Fisher Scientific) with 1 mM of phenylmethylsulfonyl fluoride and protease inhibitor cocktail. Protein concentration was evaluated through the bicinchoninic acid (Thermo Fisher Scientific) according to the provided instructions (Mazzoni et al., 2020). The OCN protein was quantified using the Human OCN Instant ELISA (Thermo Fisher Scientific) following the provided protocol (Mazzoni et al., 2020). The analysis was performed in triplicate for each experimental group.

2.15 | Statistical analysis

Statistical analyses of experiments, which were performed in triplicate, were carried out using GraphPad Prism 7.0 software for Windows. Data obtained from Alamar Blue assay, wound-healing test and Annexin V/PI were analysed with two-way analysis of variance (ANOVA) and multiple comparison tests. The *t* test was used to

analyse the OCN protein expression and matrix mineralization, whereas statistical analysis of fluorescence intensity mean was carried out using one-way ANOVA. The activated Caspase 3 expression levels measured by ELISA test was expressed their media \pm SD. A *p* < 0.05 indicates that the difference is statistically significant. In terms of data analysis of real-time PCR, the fold change (FC) for each gene expression was calculated using the $2^{-\Delta\Delta CT}$ method and then normalized by comparing these values with those of the housekeeping genes, which were used as controls. All reactions were performed in triplicate; twice fold up- or downregulated expression ($\text{Log}_2 \text{FC} > 1$ or < -1) compared to controls was considered significant.

3 | RESULTS

3.1 | Physico-chemical features of SrCPC, SrCPC-MTX and SrCPC-DOX scaffolds

The DOX or MTX drugs released on self-hardening apatitic scaffolds were investigated. In this study, SrCPC-MTX and SrCPC-DOX scaffolds were prepared to achieve release of drugs into these ranges, in fact we obtained MTX and DOX release of \sim 48 and 5 $\mu\text{g}/\text{mL}$ after 3 days, respectively (Iafisco et al., 2016). The phase composition of SrCPC was investigated before mixing the precursors and at 72 h after mixing at 37°C, exhibiting the typical diffraction patterns of α TCP and apatite, respectively (Figure 1).

To investigate the structure of the materials, SEM analysis is performed on drug-free SrCPC and doped biomaterials (SrCPC-DOX or SrCPC-MTX). The Figure 2a shows the typical microstructure of

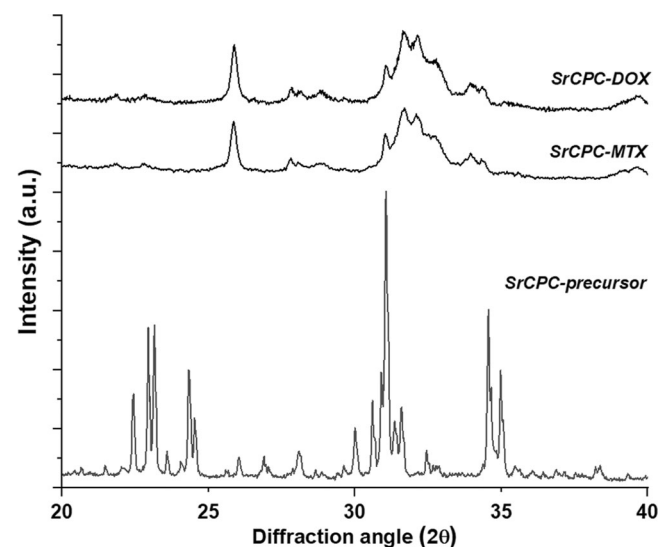


FIGURE 1 Diffraction patterns of strontium-doped calcium phosphate scaffold (SrCPC) precursor before mixing with liquid component (control). SrCPC-MTX and SrCPC-DOX patterns are investigated at 72 h after mixing. DOX, doxorubicin; MTX, methotrexate.

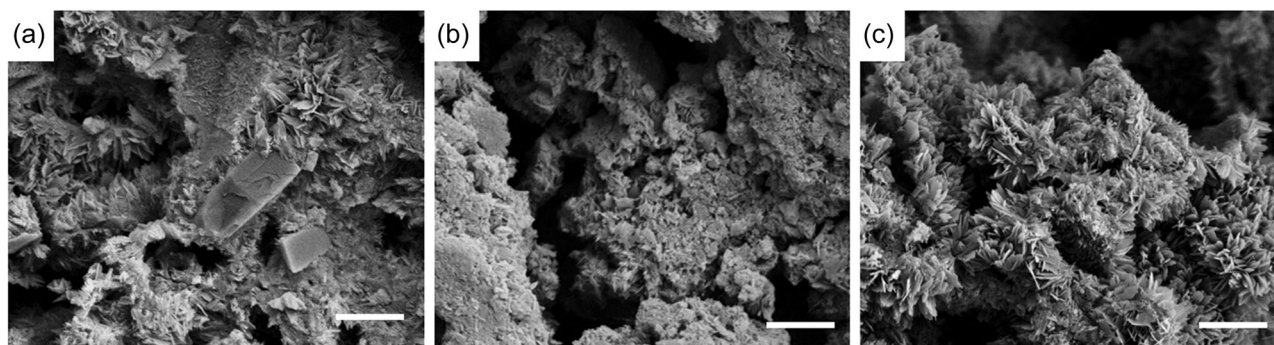


FIGURE 2 Scanning electron microscopic images of (a) drug-free strontium-doped calcium phosphate scaffold (SrCPC) (control); (b) SrCPC-DOX and (c) SrCPC-MTX. Scale bar = 1 μm . DOX, doxorubicin; MTX, methotrexate.

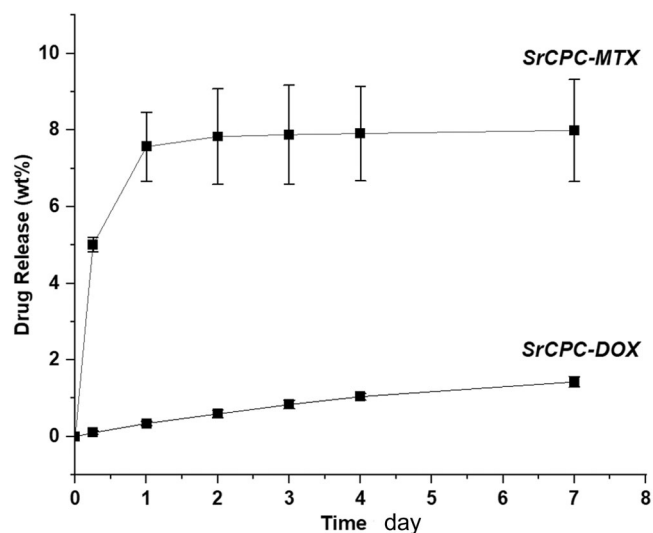


FIGURE 3 Drug release profiles for SrCPC-MTX and SrCPC-DOX up to 7 days. DOX, doxorubicin; MTX, methotrexate; SrCPC, strontium-doped calcium phosphate scaffold.

self-hardening apatitic bone cements featuring elongated interlocking nanocrystals. The comparison between the SEM images shows that the loading with DOX (Figure 2b) or MTX (Figure 2c) does not affect the structural features of the scaffold.

To characterize the materials, the drug release kinetics were analysed. The drug release profile of SrCPC-MTX and SrCPC-DOX scaffolds was performed up to 7 days (Figure 3 and Supporting Information S1: Table S1) and fits with the Korsmeyer–Peppas model (Ahmed et al., 2019; Bruschi, 2015) (Supporting Information S1: Table S2).

The SrCPC-MTX was mathematically associated to a process defined as diffusive regime with hampered release, whereas for SrCPC-DOX the release mechanism is governed by anomalous transport, that is a combination of diffusion and swelling phenomena (Bruschi, 2015). Such difference is ascribable to several factors, including the chemical nature of the drug and its interaction with the superficial end-groups exposed by the material (Sarda et al., 2018).

In particular, MTX contains a glutamic acid that can interact with the surface of nanocrystalline HA, in particular with the two carboxylate end-groups, resulting in the association with Ca^{2+} ions (Mukesh et al., 2009; Sarda et al., 2018). Conversely, DOX is characterized by an aromatic chemical structure with multiple functional groups and oxygen atoms. In the typical alkaline environment occurring during the cement setting reaction, the DOX structure exhibits hydrogen atoms linked to the $-\text{OH}$ groups and amino group with positive charge ($-\text{NH}_3^+$). In this condition, DOX has high affinity with apatite nanocrystals forming the cement matrix (Iafisco et al., 2016), thus resulting in a slower and different release kinetic.

3.2 | Cytotoxic effects of SrCPC-MTX and SrCPC-DOX on SAOS-2, SAOS-eGFP and U2-OS cell lines

The ability of SrCPC scaffolds linked to the anticancer drugs MTX (SrCPC-MTX) and DOX (SrCPC-DOX) to contrast OS cell proliferation was analysed in vitro up to Day 7. In this study, SrCPC-MTX and SrCPC-DOX scaffolds were prepared to achieve release $\sim 48.73 \pm 14.15$ and 5.18 ± 0.42 $\mu\text{g}/\text{mL}$ after 3 days, respectively. As regards drug loading concentrations, in literature there are heterogeneous data about MTX, which range from 0.1 to 100 μM (Sramek et al., 2016) to >100 μM in case of primary SAOS cell line (Sramek et al., 2016). About DOX, the tested concentration range is 10–320 μM for several three-dimensional (3D) culture, including OS cell line (U2-OS) (Baek et al., 2016).

SEM analysis was used to investigate cytotoxic effects of functionalized cements on SAOS-2 cells grown on them, up to Day 7. The effects of released drugs were assessed by evaluating cell numbers and fluorescence intensity rate and metabolic activity reductions in the engineered SAOS-eGFP cells grown on the biomaterials. SEM analysis of SAOS-2 grown on doped-scaffolds revealed that at Day 7, SAOS-2 cells were well spread and completely covered the SrCPC scaffold surface exhibiting their natural morphology and cytoplasmic extensions connecting them with the scaffold surface and each other. At Day 7, SAOS-2 cells grew almost completely on SrCPC-MTX scaffold surface (Figure 4a). However,

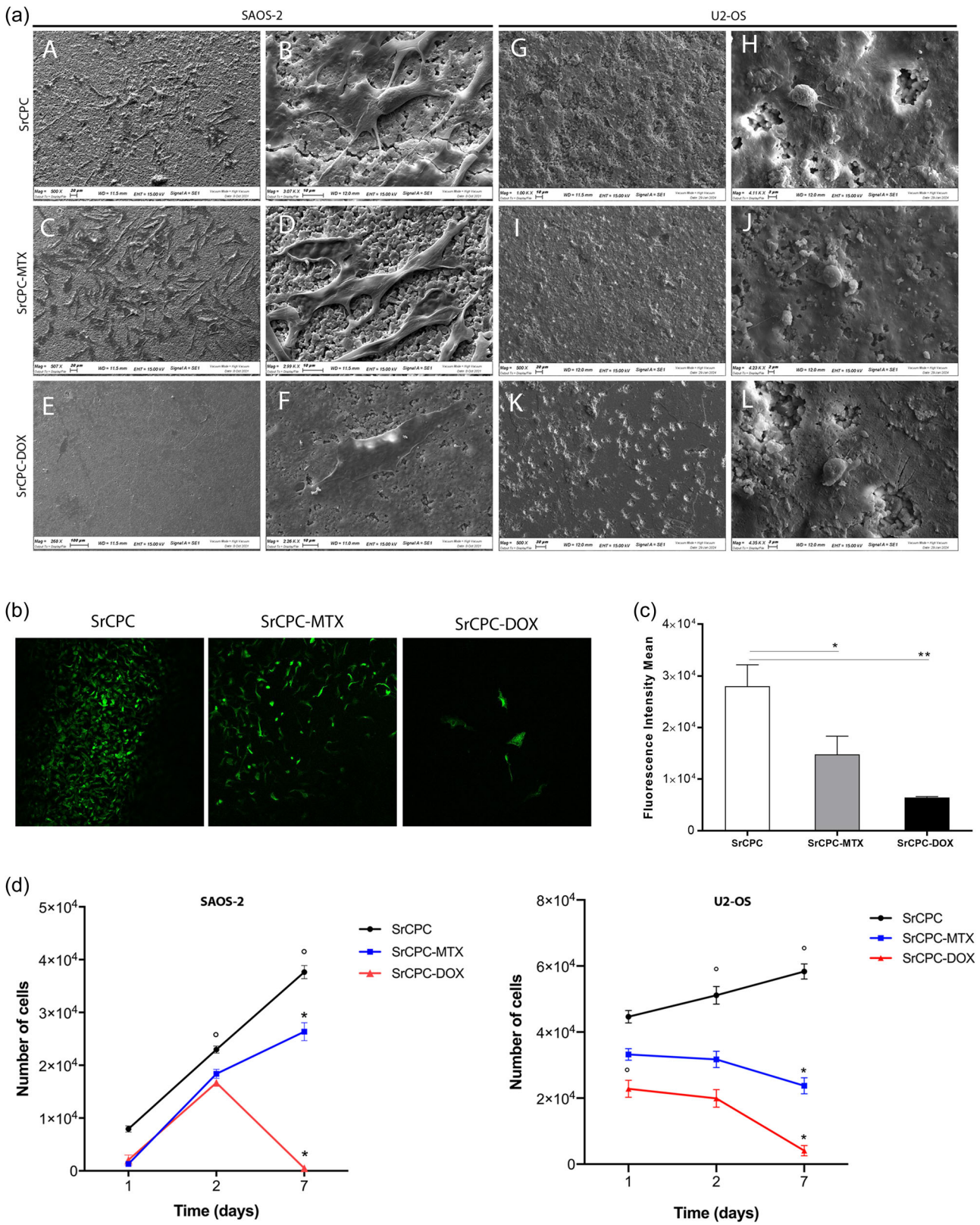


FIGURE 4 (See caption on next page).

cells growing on the drug-loaded scaffolds showed an altered morphology compared to SAOS-2 cells grown on the control. The cell culture appeared with an altered morphology evidenced by cellular swelling and scarce cytoplasmic bridges among cells. Contrariwise, SrCPC-DOX did not allow SAOS-2 cells to cover the scaffold surface. In this instance, only a few cells with an altered morphology were visible on the scaffold surface (Figure 4a). These results indicate that SrCPC-MTX and SrCPC-DOX scaffolds displayed a cell-killing effect on SAOS-2 cells compared to SrCPC. Microscopic analyses verified that the drug-free SrCPC scaffold surface was completely covered with SAOS cells, with unaltered morphology. Contrariwise, SAOS cells in contact with SrCPC-MTX presented an altered morphology. Furthermore, only a few SAOS cells were observed on the SrCPC-DOX scaffold. U2-OS cells grown on scaffolds, visualized on SEM, appear with rounded morphology. U2-OS cells completely covered the SrCPC scaffold surface exhibiting their cytoplasmic extensions connecting them with the scaffold surface and each other, while U2-OS cells grown on doped scaffolds appear to lose their extracellular extrusions (Figure 4a).

We assessed in vitro the ability of drug-loaded SrCPC scaffolds to contrast OS cell proliferation using the SAOS-eGFP cell line, which represents an appropriate study model, as previously reported (Manfrini et al., 2015; Morelli et al., 2007). The effects of SrCPC-MTX and SrCPC-DOX scaffolds, on SAOS-eGFP cells viability, were investigated by evaluating the fluorescence intensity emitted by the engineered cell line, at Day 7. Digital images obtained using a confocal microscope revealed that SrCPC scaffold was completely covered by SAOS-eGFP cells (Figure 4b). Indeed, the number of SAOS-eGFP cells decreased in SrCPC-MTX and cells were mostly absent in SrCPC-DOX (Figure 4b), confirming the SEM analysis. Quantification of fluorescence intensity confirmed the data from the confocal microscope. The fluorescence intensity means of SAOS-eGFP cells grown on SrCPC scaffold was higher than cells grown on SrCPC-MTX ($p < 0.05$) and SrCPC-DOX ($p < 0.005$). There were no statistical differences between SrCPC-MTX and SrCPC-DOX groups (Figure 4c). These data were supported by qualitative and quantitative results obtained by fluorescence analysis of engineered SAOS-eGFP cells. Indeed, images from confocal microscopy analysis and

measurement of fluorescence intensity revealed a reduced number of cancer cells grown on SrCPC-MTX compared to the control (52%) and a higher decrease of SAOS-eGFP cells grown on SrCPC-DOX scaffold (28%). The effects of SrCPC-MTX and SrCPC-DOX scaffolds on metabolic activity of SAOS-2 and U2-OS cells were investigated using Alamar Blue assay, at Day 1, 2 and 7. Metabolic activity showed an increasing number of SAOS-2 cells grown on the control drug-free SrCPC, up to Day 7. Contrariwise, SAOS-2 cells increased their number in SrCPC-MTX and SrCPC-DOX during the first 2 days of culture, then decreased, at Day 7 (Figure 4d; $p > 0.05$). At Day 7, the number of SAOS-2 cells significantly decreased in MTX/DOX-conjugated scaffolds compared to the control ($p < 0.005$ and $p < 0.001$, respectively) (Figure 4d). The SrCPC-DOX material induced a complete cytotoxic effect detectable as the absence of cells on the material, evidenced by the Alamar Blue assay (Figure 4d). U2-OS cells increased their number in SrCPC material until Day 7 ($p < 0.05$). Cell proliferation of U2-OS cells grown on SrCPC-MTX and SrCPC-DOX decreased at Day 2. Then, at Day 7, the number of U2-OS cells significantly decreased in MTX/DOX-conjugated scaffolds compared to the control (Figure 4d; $*p < 0.05$).

3.3 | Apoptosis/necrosis process in SAOS-2 and U2-OS cells grown on SrCPC-DOX and on SrCPC-MTX

To test the potential to induce apoptosis of the doped materials on the SAOS-2 and U2-OS culture, three different methods were employed. Apoptosis is a form of programmed cell death that initiated by a tightly regulated signalling cascade, which results in caspase activation. To gain insights into the putative mechanism of SrCPC-DOX- and SrCPC-MTX-induced cell death, OS cell cultures were grown on scaffolds for 4 days. Activated Caspase-3/7 expression proteins were visualized in both OS cell lines grown on SrCPC-DOX scaffold. Indeed, the Caspase-3/7-specific fluorochrome detection dye revealed significantly higher levels of caspase 3/7-positive cells (green) in the OS cells grown on SrCPC-DOX compared to SrCPC-MTX. The expression of Caspase-3/7 proteins was lower in

FIGURE 4 Cytotoxic effects of SrCPC-MTX and SrCPC-DOX on OS cell lines. (a) Scanning electron microscopic (SEM) analysis. SAOS and U2-OS cells grown on strontium-doped calcium phosphate (SrCPC) scaffold exhibiting normal morphology and cytoplasmic extensions. (A) Scale bar: 20 μm , $\times 500$, (B) scale bar: 10 μm , $\times 3.07\text{K}$, (G) scale bar: 10 μm , $\times 1.00\text{K}$, (H) scale bar: 3 μm , $\times 4.11\text{K}$. OS cell lines grown on SrCPC-MTX scaffold exhibiting a damaged morphology; (C) scale bar: 20 μm , $\times 507$, (D) scale bar: 10 μm , $\times 2.99\text{K}$, (I) scale bar: 20 μm , $\times 500$, (j) scale bar: 2 μm , $\times 4.23\text{K}$. In the same way, the few OS cell lines grown on SrCPC-DOX scaffold showing a impaired morphology; (e) scale bar: 100 μm , $\times 268$, (F) scale bar: 10 μm , 2.26 KX, (K) scale bar: 30 μm , $\times 500$, (L) scale bar: 3 μm , $\times 4.35\text{K}$. (b) Images acquired with confocal microscope of SAOS-eGFP cells on SrCPC, SrCPC-MTX, SrCPC-DOX. Z-stack images were collected at 0.5 μm slices by confocal microscopy from the bottom to the top of the cells and were merged into a single frame. (c) Quantification of SAOS-eGFP cells fluorescence intensity with ImageJ software, SrCPC versus SrCPC-MTX, $*p < 0.05$; SrCPC versus SrCPC-DOX ($**p < 0.005$). (d) Graph shows increasing number of SAOS-2 cells grown on SrCPC up to Day 7 ($p > 0.05$). SAOS-2 cells increased on SrCPC-MTX and SrCPC-DOX up to Day 2 ($p > 0.05$), whereas decreased on SrCPC-MTX and SrCPC-DOX up to Day 7 ($p < 0.05$). Significant differences were revealed between SrCPC-MTX scaffold and activated at Day 7 ($*p < 0.001$). In the same way, U2-OS cells grown on SrCPC showed an increase of cell proliferation up to Day 7 ($p < 0.05$), while U2-OS grown on SrCPC-MTX and SrCPC-DOX exhibited a significant decrease of cell proliferation at day 7 ($p < 0.05$). The doped scaffolds show a statistically significant decrease, in terms of cell proliferation, at Day 7 compared to the control material ($*p < 0.01$). DOX, doxorubicin; MTX, methotrexate.

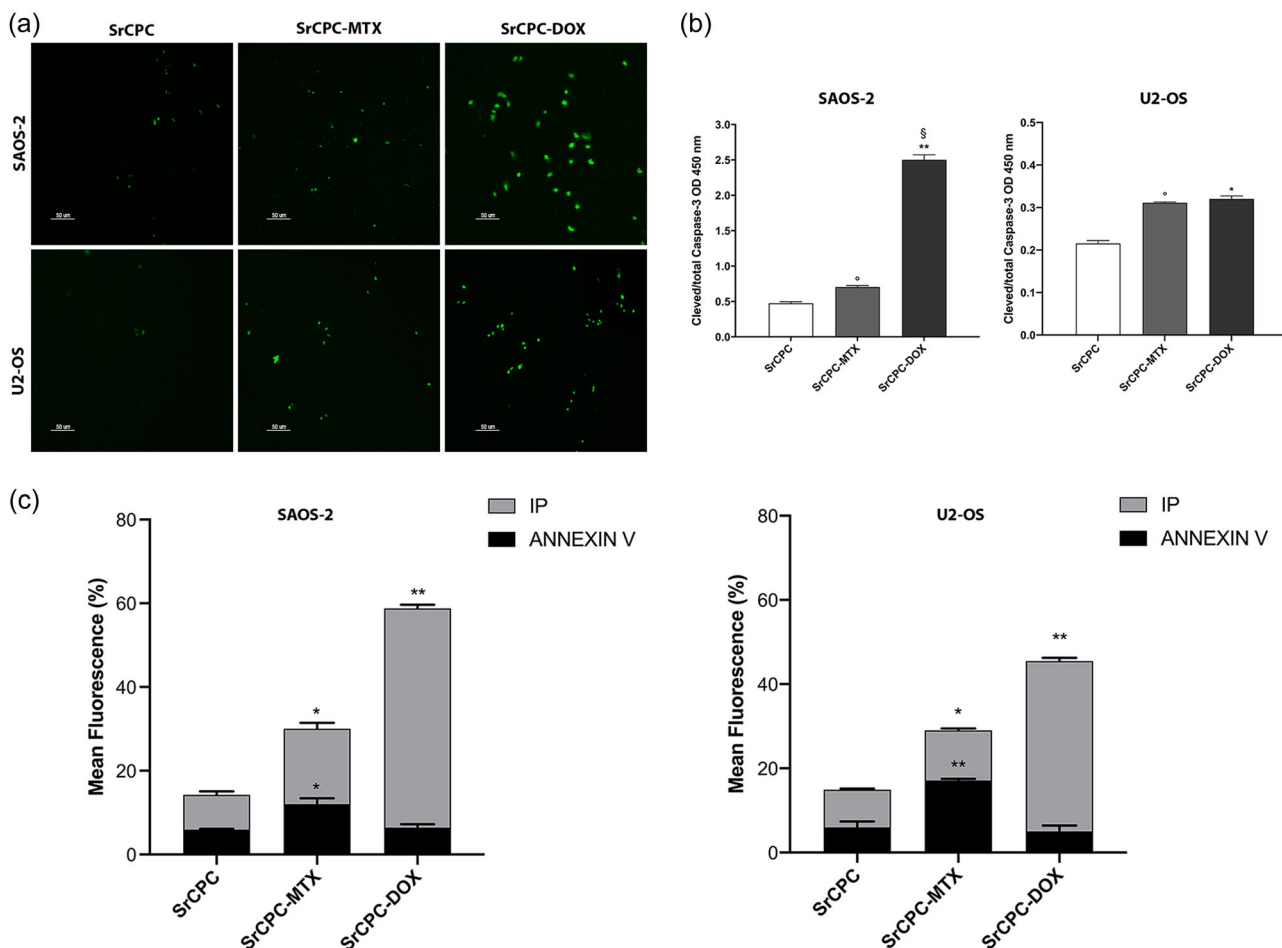


FIGURE 5 Evaluation of induction of apoptosis/necrosis in SAOS-2 and U2-OS grown on strontium-doped calcium phosphate scaffold (SrCPC), SrCPC-MTX and SrCPC-DOX scaffolds. (a) Immunostaining of activated caspase 3/7 in SAOS-2 and U2-OS cells grown on SrCPC, SrCPC-MTX and SrCPC-DOX scaffolds. (b) Quantification of protein expression of cleaved Caspase-3 on SAOS-2 ($p < 0.05$; $**p < 0.0001$) and U2-OS ($*p < 0.01$; $*p < 0.001$) compared to control (SrCPC). A statistical increase of cleaved caspase 3 was revealed in SAOS grown on SrCPC-DOX scaffolds compared to SrCPC-MTX ($^{\S}p < 0.0001$). Data are shown as mean \pm SD. $n = 3$. (c) SAOS-2 and U2-OS grown on SrCPC-MTX and SrCPC-DOX scaffolds showed a positive for Annexin V/propidium iodide (PI) staining at Day 4, compared to control ($*p < 0.01$; $**p < 0.0001$). DOX, doxorubicin; MTX, methotrexate.

OS cells grown on drug-free SrCPC, compared to other experimental groups (Figure 5a).

The quantification of cleaved caspase-3 protein reveals the apoptosis process induced in SAOS-2 and U2-OS cells grown on SrCPC-DOX and SrCPC-MTX for 4 days (Figure 5b). The ELISA testing revealed significantly higher levels of cleaved caspase-3 protein in SAOS-2 culture grown on SrCPC-MTX, which induced a significant increase of cleaved caspase-3 protein expression expressed as (mean \pm SD) (0.705 ± 0.021), compared to control represented by SrCPC ($0.475 \text{ OD} \pm 0.021$) ($p < 0.05$) and TCPS ($0.163 \text{ OD} \pm 0.014$). The material SrCPC-DOX, presented a higher OD level ($2.502 \text{ OD} \pm 0.07 \text{ SD}$) compared to controls, that is, SrCPC and TCPS (Figure 5b). In U2-OS cells, quantification of caspase 3 highlighted a statistically significant increase in its activation in cells cultured on both materials, SrCPC-MTX and SrCPC-DOX, compared to the control. U2-OS cells, cultured on doped-scaffolds, showed similar active caspase 3 protein levels (Figure 5b).

Annexin V-positive staining was detected in both OS cells grown on SrCPC-MTX material compared to SrCPC-DOX and control (Figure 5). Conversely, the SrCPC-DOX material seems to induce a higher necrotic effect in both OS cell lines highlighted by the IP positivity compared to SrCPC-MTX and control (Figure 5c).

3.4 | Cell migration ability in SAOS-2 and U2-OS cells grown on SrCPC-DOX and SrCPC-MTX

Both OS cell lines, seeded on SrCPC-DOX- and SrCPC-MTX-doped biomaterials, showed a reduction in migratory capacity and a significant increase in wound area up to 72 h, compared to the control (SrCPC). SrCPC-DOX reduces the migratory capacity more significantly than SrCPC-MTX at 48 and 72 h of SAOS-2, as well as at 24 and 72 h of U2-OS (Figure 6).

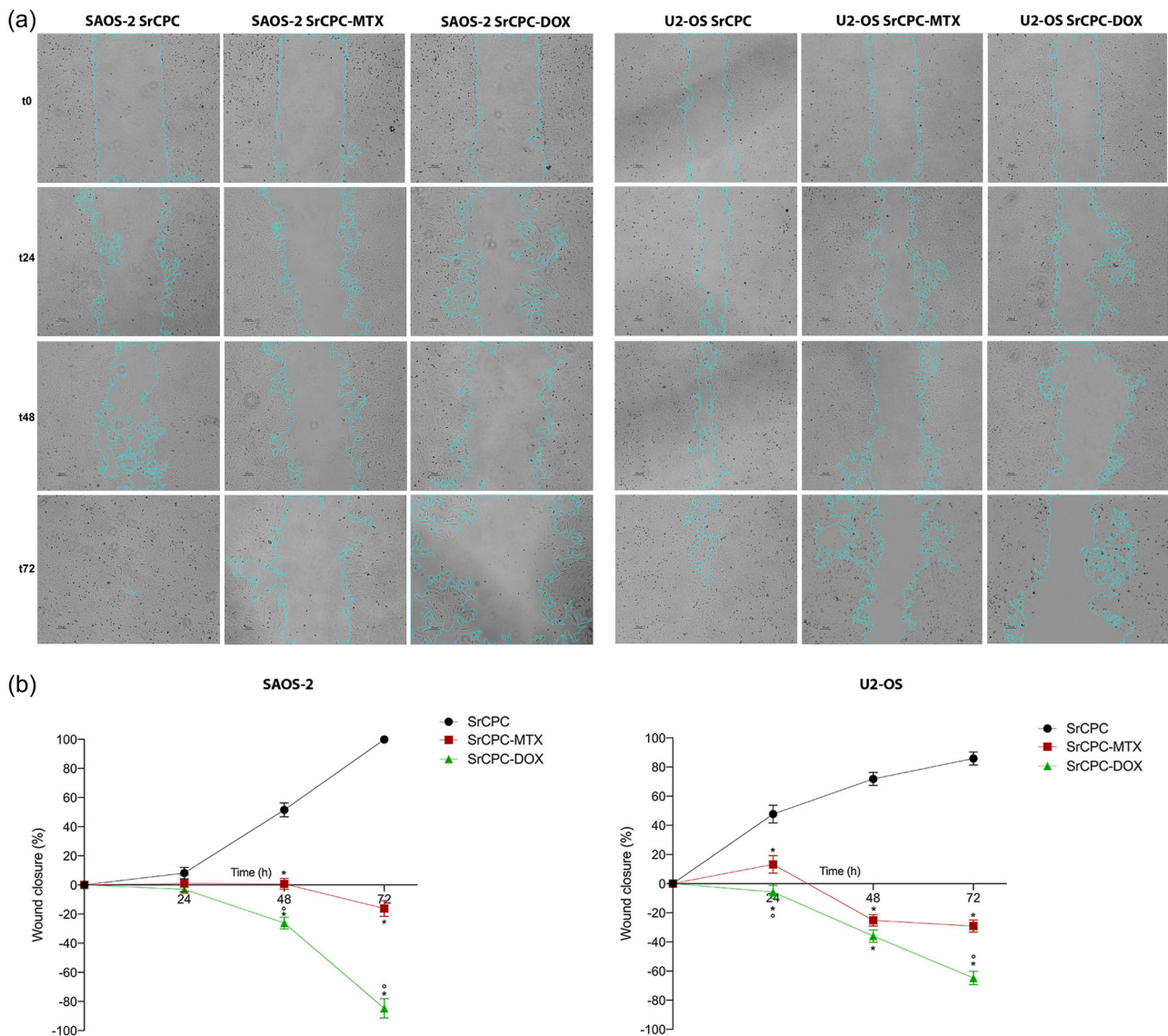


FIGURE 6 Effects of strontium-doped calcium phosphate scaffold (SrCPC), SrCPC-MTX and SrCPC-DOX on SAOS-2 and U2-OS migration ability. (a) Wound-healing assay on SAOS-2 and U2-OS at 24, 48 and 72 h. The wound closure rate was measured by detecting the closure distance. Osteosarcoma (OS) cell lines grown on SrCPC were used as a control. Representative micrographs under a phase contrast microscope are shown. Scale bar, 50 μ m. (b) Quantification of wound gap distance. Data are presented as the mean \pm SD ($n = 3$). A statistical significant difference was revealed between (i) SrCPC versus SrCPC-DOX and SrCPC versus SrCPC-MTX ($*p < 0.0001$) and (ii) SrCPC-DOX versus SrCPC-MTX ($*p < 0.001$) at each timepoint of analysis. DOX, doxorubicin; MTX, methotrexate.

3.5 | Cytocompatibility proprieties of SrCPC scaffold

The cytocompatibility of no-doped scaffold (SrCPC) was analysed using human ASCs grown on SrCPC scaffold and in TCPS (the control). Specifically, SEM, metabolic activity, Live/Dead and cytoskeleton architecture analyses were carried out in the two experimental groups at different time points, as reported below (Figure 7).

The microstructure and morphology of SrCPC scaffold with and without hASCs grown on them, up to Day 14, were SEM analysed at higher magnification ($\times 80$ – $4.00K$) (Figure 7a). hASCs grown on the

scaffold showed a normal cell morphology, exhibiting pseudopodium-like structures, which connect them to the biomaterial surface (Figure 7a). Indeed, as indicated by the arrows, human stem cells are able to adhere to undoped material. The SrCPCs, studied herein, present a granular structure offering a good microenvironment for adhesion and proliferation of hASCs, as shown by SEM analysis where cells grew well on the scaffold surface.

Live/Dead assay was used to analyse the cell viability of hASCs grown on the scaffold and TCPS, at Day 3, 6 and 14. Cyto-dye, a green fluorescent dye, and PI, a red fluorescent dye, were used to stain live and dead cells, respectively. At each experimental

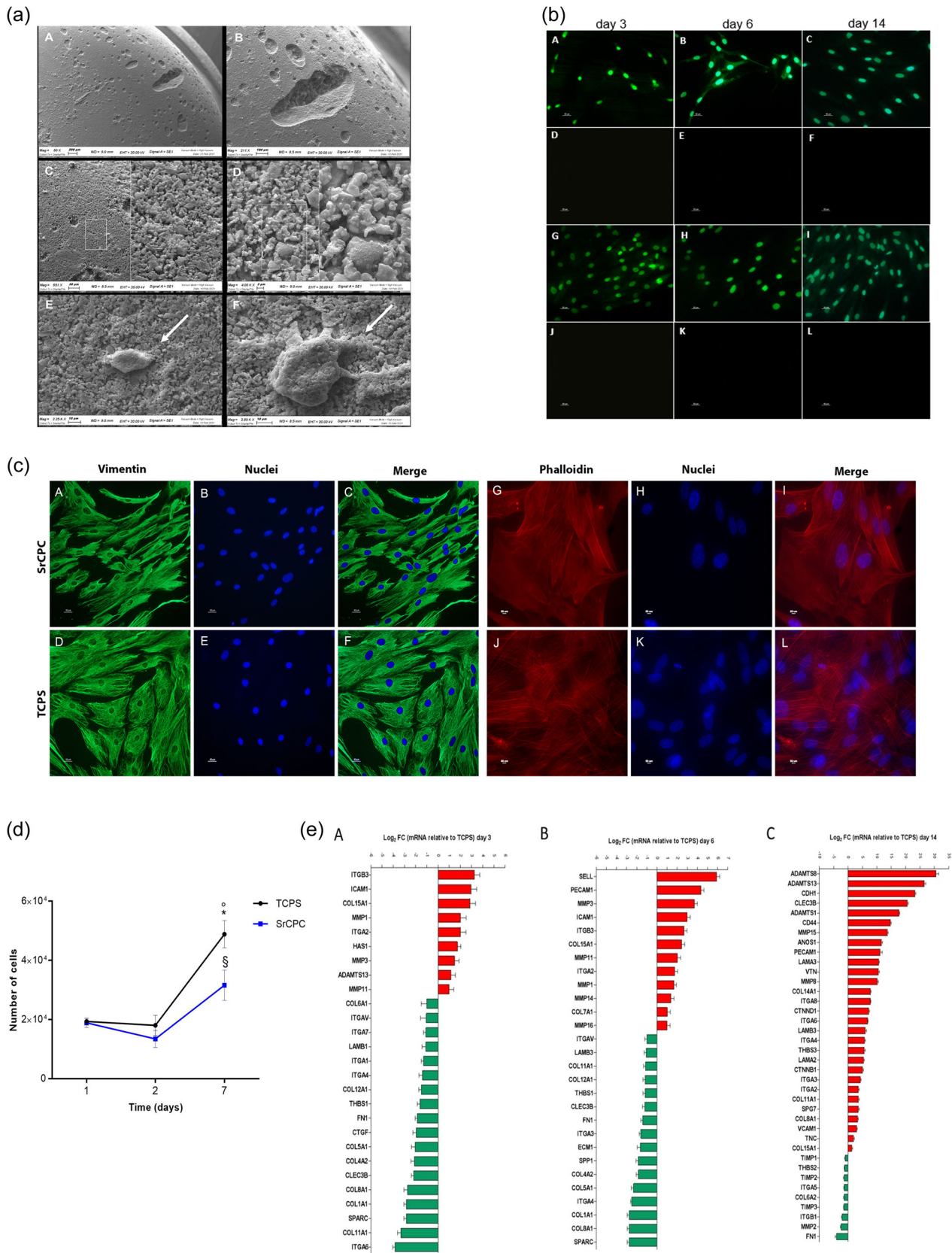


FIGURE 7 (See caption on next page).

time point, carried out on hASCs grown in contact with the scaffold, digital images showed the presence of live cells, which were indistinguishable from those grown on the control. Dead cells were no detected (Figure 7b). In addition, live cells were identified in the scaffold using confocal microscope in slices (z) of 0.5 μm , at Day 3, 6 and 14 showing a time dependent increase. These data demonstrate the cytocompatibility of the SrCPC scaffold.

The cytoskeleton architecture of hASCs grown on the SrCPC scaffold and TCPS, was analysed by performing phalloidin-TRITC staining, at Day 14 (Figure 7c). The cytoskeleton showed a well-organized structure with actin filaments being distributed uniformly in the cell cytoplasm, at Day 14, in hASCs grown on scaffold and TCPS, demonstrating that the scaffold had not influence on the cytoskeleton architecture, up to Day 14. In the digital images at $\times 40$ magnification (Figure 7c), actin filaments appear unaltered, confirming the cytocompatibility of the SrCPC scaffold. The cytocompatibility of the undoped-scaffold was investigated by highlighting the cytoskeletal protein vimentin in hASC cultures. The vimentin intermediate filaments appear regular and well distributed in the cells, thus confirming the cytocompatibility of the scaffold (Figure 7c).

Alamar Blue assay was carried out to analyse the effects of the scaffold on hASCs cells viability. Cell metabolic activity of each time point was converted into the number of viable cells by calculating the interpolated X value of hASCs calibration curve. Results showed an increase cell number of hASCs grown on the SrCPC scaffold and TCPS, up to Day 7 (Figure 7d). At Days 1 and 2, there were no significant differences between the two experimental groups (Figure 7d; $p > 0.05$). Contrariwise, there are statistical differences in hASCs grown on the SrCPC scaffold compared to hASCs grown on TCPS, at Day 7 (Figure 7d; $p < 0.05$). Nevertheless, SrCPC scaffold induced hASCs growth and did not cause any cytotoxicity.

3.6 | SrCPC scaffold modulate the ECM and adhesion molecules expression in hASCs

The ECM and adhesion molecules gene expression profiles were investigated using PCR array technology in hASCs cultured on the SrCPC scaffold and TCPS to evaluate the scaffold cytocompatibility. Analyses were carried out at Day 3, 6, and 14 (Figure 7e and Supporting Information S1: Tables S4–S6). At Day 3, a total of 27 differentially expressed genes, including nine upregulated genes ($>1 \log_2 \text{FC}$; $p < 0.05$; red) and 18 downregulated genes ($<-1 \log_2 \text{FC}$; $p < 0.05$; green), were identified in hASCs grown on scaffold, compared to the control, as reported in Supporting Information S1: Table S2–S4. Cellular biology results were supported by molecular genetic/biology data, such as gene expression analysis carried out using a PCR array technique to evaluate the ECM and cell adhesion molecules profile. In bone, the ECM regulates cell adhesion, proliferation and differentiation, producing collagen, integrin, fibronectin and connective tissue growth factor (Ren et al., 2011). Moreover, osteogenic differentiation during the ECM secretion phase in MSCs induces morphological changes in immature osteoblasts, immediately followed by the formation of mature osteoblasts (Paiva & Granjeiro, 2017). In hASCs, genes encoding cell adhesion molecules were upregulated in the presence of SrCPC scaffold, demonstrating the ability of the scaffold to mediate cell-cell and/or cell-scaffold interactions. Among them, ICAM1, PECAM1, VCAM1, SELL and CD44 molecule upregulation was observed. SELL is a calcium-dependent lectin that mediates cell adhesion by binding to glycoproteins on neighbouring cells (Wedepohl et al., 2017), whereas CD44 molecule is responsible for cell-cell interactions engaging ECM components, such as hyaluronan, collagen, growth factors, cytokines or proteases (Midgley et al., 2013). ECM-cell interaction is crucial for tissue morphogenesis and architecture, thus such actions are mediated by integrin and cadherin (Di Benedetto et al., 2015).

FIGURE 7 Characterization of vitality and proliferation of human adipose derived-mesenchymal stem cell (hASC) grown on strontium-doped calcium phosphate (SrCPC) scaffold. (a) Scanning electron microscopy analysis of SrCPC scaffold. The biomaterial consists of a nanostructured calcium-deficient hydroxyapatite (HA) substituted with strontium. The structure of scaffold was observed at different magnification, Scale bar: 200 μm , $\times 80$; scale bar: 100 μm , $\times 211$; scale bar: 200 μm , $\times 651$; scale bar: 3 μm , $\times 4.00\text{K}$, respectively (A–D). hASCs (white arrows) on the substrate exhibited cytoplasmic bridges, with a normal morphology; scale bar: 10 μm , $\times 2.25\text{K}$; scale bar: 10 μm , $\times 2.85\text{K}$, respectively (E, F). (b) Cell viability analysis of hASCs using Live/Dead assay. Live cells (hASCs) grown in contact with SrCPC at Day 3, 6, 14 (A–C). Dead cells were no detected (D–F). Live cells (hASCs) grown on tissue culture polystyrene (TCPS) at Day 3, 6, 14 (G–I). Dead cells were no detected (J–L). Scale bar: 100 μm . (c) Cytoskeleton analysis of hASCs grown on the SrCPC scaffold. The expression of vimentin protein and actin filaments do not show alteration in the structural organization in hASCs grown on SrCPC, compared to control (TCPS). Magnification $\times 20$ (A–F) and $\times 40$ (G–L). Scale bar for each magnification: 50 μm . Cellular nuclei were stained with 0.5 mg/mL 4',6-diamidino-2-phenylindole (DAPI). (d) hASCs metabolic activity measured by Alamar Blue assay at Days 1, 2 and 7. Graph shows increasing number of hASCs grown on SrCPC scaffold ($p < 0.05$) and on TCPS ($p < 0.05$) up to Day 7. Significant differences were revealed between SrCPC scaffold and TCPS at Day 7 ($p < 0.05$). (e) Extracellular matrix and adhesion molecules genes modulated by SrCPC scaffold in hASCs. (A) At 3 days $n = 27$ differentially expressed genes, including nine upregulated genes ($>1 \log_2 \text{fold change [FC]}$; $p < 0.05$; red) and 18 downregulated genes ($<-1 \log_2 \text{FC}$; $p < 0.05$; green), were identified in hASCs grown on scaffold compared with control. (B) At Day 6, $n = 28$ differentially expressed genes, including 12 upregulated genes ($>1 \log_2 \text{FC}$; $p < 0.05$; red) and 16 downregulated genes ($<-1 \log_2 \text{FC}$; $p < 0.05$; green), were identified in hASCs grown on scaffold compared with control (TCPS). (C) At Day 14, 38 differentially expressed genes, including $n = 29$ upregulated genes ($p < 0.05$; red) and $n = 9$ downregulated genes ($p < 0.05$; green), were identified in hASCs grown on scaffold compared with control. DOX, doxorubicin; MTX, methotrexate.

The SrCPC scaffold stimulated the upregulation of genes encoding integrins and cadherins in hASCs. Early expressed integrins are ITGA2 and ITGB3 followed by ITGA3/4/6/8, which were upregulated up to Day 14. The gene expression levels of ITGA2 and ITGA3 were in agreement in the two different PCR-Array for ECM and Osteogenesis, as well as ITGA1, which resulted downregulated in both assays, at the first time point. Of all, the cadherin CDH1, a calcium-dependent cell adhesion protein, resulted upregulated in hASCs grown on the biomaterial. Integrins and cadherins have an important role in proper development, function, regeneration of skeletal tissue and MSCs osteogenic differentiation (Di Benedetto et al., 2015; Docheva et al., 2014). Collagen is the most abundant constituent of the ECM acting as a mechanical support for cells (Saito & Marumo, 2015). In vitro results demonstrated that the SrCPC scaffold promoted the expression of genes encoding for collagen proteins including COL7/8/11/14/15A1. The latter is constantly up-expressed during the experimental time course in both the PCRs assay thus highlighting its important role in osteogenic differentiation and mineralization (Wu et al., 2020). Matrix metalloproteinases (MMPs), with the ability to cleave collagens and proteoglycans, are among the most active proteases in ECM regulation (Paiva & Granjeiro, 2017). Such proteinases are involved in wound healing and tissue remodelling (Milner & Cawston, 2005). *MMP1/3/11* gene expression was promptly induced by SrCPC in hASCs. *MMP8/15* were positively modulated by the scaffold later. Indeed, while *MMP15* is a membrane-type metalloproteinase (Liang et al., 2016), *MMP8* is expressed in osteoblastic progenitors, differentiated osteoblasts, and osteocytes (Sasano et al., 2002). Moreover, *MMP10*, which is essential for human bone development (Bord et al., 1998) and takes part in the physiological processes of bone growth (Ortega et al., 2004), resulted positively modulated by the SrCPC scaffold.

3.7 | SrCPC material induces the osteogenic differentiation in hASCs

In the second phase of our study, the effect of SrCPC scaffold in the osteogenic differentiation were assessed employing hASC cultures. Matrix mineralization, OCN protein expression and osteogenic genes expression were investigated in hASCs grown on the scaffold, up to day 14 (Figure 8a–d and Supporting Information S1: Tables S7–S9). Alizarin Red staining was used to evaluate the mineralized matrix in hASCs grown on SrCPC scaffold and TCPS in basal medium. Cell cultures for the two experimental groups were stained with alizarin red and imaged using a bright-field microscope. Digital images show that SrCPC scaffold promotes mineral matrix deposition differently compared to TCPS (Figure 8a). Afterwards, alizarin red staining was eluted to perform optical density measurements. Results showed an increased calcified matrix in hASCs grown on the SrCPC scaffold compared to TCPS ($p < 0.0001$; Figure 8b), at Day 14.

OCN protein expression in hASCs grown on SrCPC scaffold and TCPS, up to day 14, were analysed using ELISA test. In hASCs grown on SrCPC the assay revealed 38.25 ng of OCN/ μ g of proteins and

17.95 ng of OCN/ μ g of proteins, in TCPS. Data show a significant increase of OCN protein expression in hASCs grown on the scaffold compared to control ($p < 0.0001$; Figure 8c).

In this study, osteogenesis RT² Profiler PCR Array was used to investigate the differentially expressed genes in hASCs grown on SrCPC scaffolds, at Day 3, 6 and 14 (Figure 8d). Results of experimental replicates obtained at Day 3 revealed the ability of the scaffold to upregulate ($>1 \log_2$ FC; $p < 0.05$; red) different genes involved in skeletal development, as reported in Supporting Information S1: Table S5–S7. In summary, in hASCs the scaffold strengthened the expression of those genes implicated in ossification, osteoblast differentiation, and bone mineralization during the experimental time course, whereas the modulation of genes involved in cell adhesion process decreased over time, up to Day 14. The *BMP2* gene resulted upregulated in our experiments suggesting hASCs osteogenic differentiation upon contact with the scaffold. Further, it has been reported that *MMP10* enhances BMP-2-induced osteoblast differentiation in vitro (Reyes et al., 2018). The crucial signalling pathways leading MSCs towards osteogenesis differentiation are *transforming growth factor- β* (*TGF- β*) and bone morphogenetic protein (BMP) (Lanzillotti et al., 2021; Mazziotta et al., 2021). Our results demonstrate that SrCPC scaffold upregulated genes are involved in these two signalling cascades. Specifically, three of the most important BMPs, involved in osteogenesis, that is, *BMP2/4/7*, resulted upregulated alongside other BMP signalling like *BMPR1A*, *BMPR2* and *SMAD5* (Martini et al., 2020). On the other hand, among factors involved in the *TGF- β* cascade, *TGFBR1/2* were positively regulated by the scaffold. The activation of cited signalling pathways leads to the expression of master osteogenic transcription factors, such as *RUNX2* and *Osterix* (*OSX*), also known as *SP7*. More precisely, *OSX* is a downstream *RUNX2* gene (Iaquinta et al., 2021a). Our results are in agreement with previous reports in as much as they demonstrated that the *RUNX2* gene was upregulated at Days 3 and 6, whereas *SP7* expression with high FC is observed at Day 14, when *RUNX2* modulation disappears (Iaquinta et al., 2021a). Finally, *RUNX2* and *SP7* activity results in specific osteoblast gene expression of including OCN and collagen (Iaquinta et al., 2021a). SrCPC biomaterial induced OCN upregulation in term of gene (*BGLAP*) and protein (OCN) expressions. In agreement, matrix mineralization analysis showed an increase matrix deposition in hASCs grown on the scaffold, as well as the upregulation of *ALPL* gene. Other osteogenic genes involved in the skeletal development process were modulated in hASCs by the scaffold. Of these, upregulation of *GLI1* and epidermal growth factor receptor (*EGFR*) was observed. *GLI1* is a transcriptional activator involved in signalling-mediated specification for osteoblast lineage inducing early osteoblast differentiation (Hojo et al., 2012). On the other hand, *EGFR* take part in *EGFR/ERK/IGFBP-3* signalling pathway inducing osteoblast differentiation and maturation (Mazzoni et al., 2020). Additionally, *CLEC3B* (Larsen et al., 2010) gene was found to be expressed in hASCs grown on the biomaterial, up to Day 14. It is well known that when MSCs differentiate into osteoblasts many osteoclast-associated cytokines are secreted, including colony stimulating factor (CSF), *receptor*

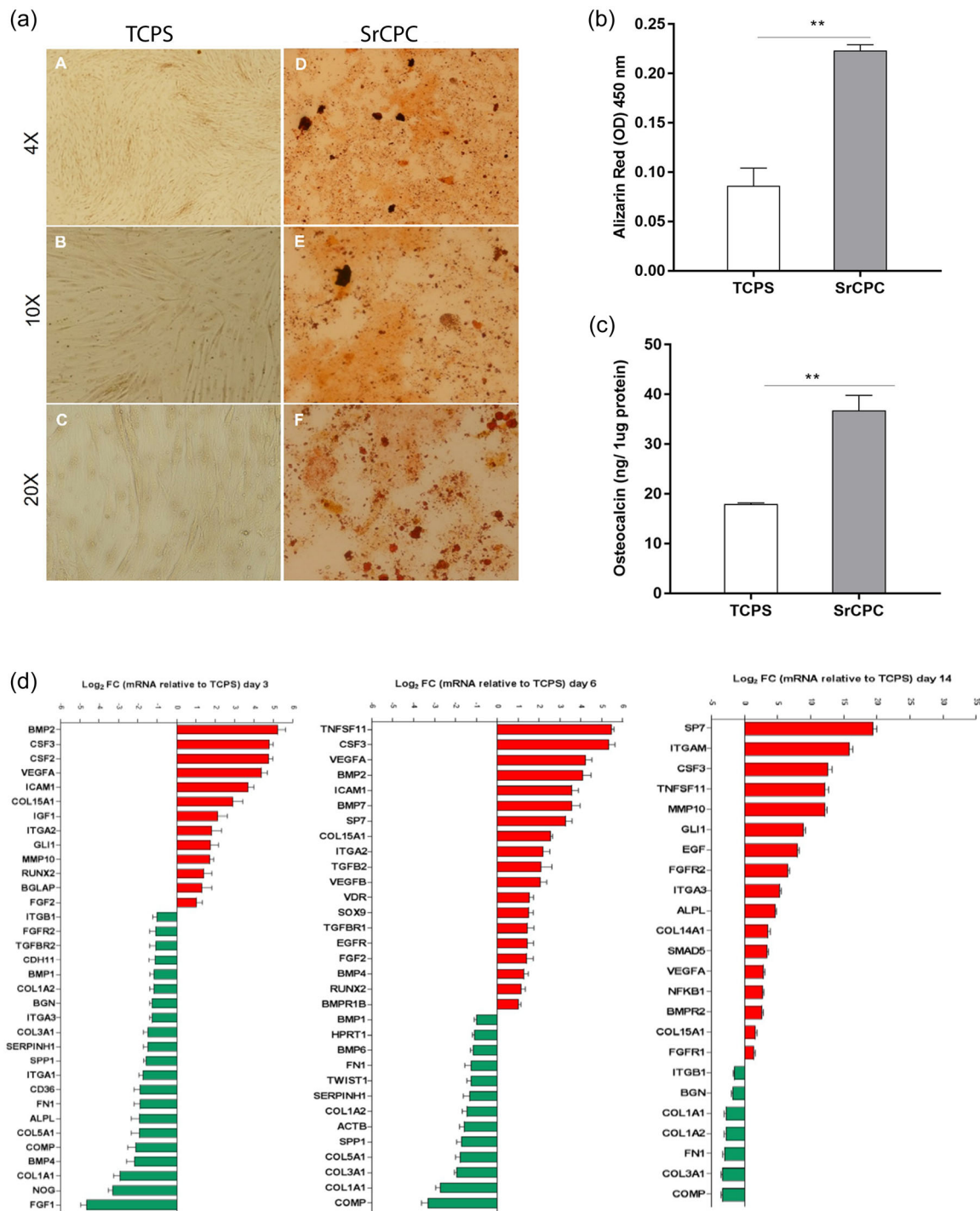


FIGURE 8 Osteoinductivity properties of strontium-doped calcium phosphate (SrCPC) scaffold evaluated with human adipose derived-mesenchymal stem cell (hASC) culture. (a) Alizarin red staining in hASCs grown on tissue culture polystyrene (TCPS) and SrCPC at $\times 4$ (A, D), $\times 10$ (B, E) and $\times 20$ (C, F) magnifications. Scale bar for each magnification: 100 μm . (b) Quantification of Alizarin Red staining through spectrophotometric analysis at 450 nm wavelength measured in hASC grown on control and SrCPC (** $p < 0.0001$). (c) OCN protein expression quantified using enzyme-linked immunosorbent assay (ELISA) test in hASCs grown on SrCPC scaffold and on TCPS at Day 14 (** $p < 0.0001$). (d) Osteogenic genes expression (messenger RNA) modulated by SrCPC scaffold in hASCs at Day 3, 6 and 14. (d) At Day 3, 34 differentially expressed genes, including 13 upregulated genes (>1 log₂ fold change [FC]; $p < 0.05$; red) and 21 downregulated genes (<-1 log₂ FC; $p < 0.05$; green), were identified in hASCs grown on scaffold compared with control. At Day 6, 32 differentially expressed genes, including 19 upregulated genes (>1 log₂ FC; $p < 0.05$; red) and 13 downregulated genes (<-1 log₂ FC; $p < 0.05$; green), were identified in hASCs grown on scaffold compared with control. At Day 14, 24 differentially expressed genes, including 17 upregulated genes (>1 log₂ FC; $p < 0.05$; red) and seven downregulated genes (<-1 log₂ FC; $p < 0.05$; green), were identified in hASCs grown on scaffold compared with control.

activator of nuclear factor κ -B ligand (RANKL) stimulating osteoclasts differentiation (Meng et al., 2020). Our experiments revealed the upregulation of *TNFSF11*, also known as RANKL, and *CSF2/3* genes. Thus, in hASCs the mechanism of bone resorption is activated together with the bone formation process. The coupled mechanisms continuously lead to bone remodelling.

4 | DISCUSSION

The effects of DOX or MTX drugs released on self-hardening apatitic scaffolds were investigated on SAOS-2, SAOS-eGFP and U2-OS cells, particularly analysing the putative mechanisms of cell death induced in *in vitro* model of SAOS-2 and U2-OS. In particular, we assessed *in vitro* the ability of drug-loaded SrCPC scaffolds to contrast OS cell proliferation, using the SAOS-2 and U2-OS cell lines, which represent appropriate study models, as previously reported (Chen et al., 2019; Morelli et al., 2007; Sarda et al., 2018; Suksiriworapong et al., 2018).

In this study, SrCPC-MTX and SrCPC-DOX scaffolds were prepared to achieve release of drugs into these ranges; in fact, we obtained MTX and DOX release of \sim 48 and 5 μ g/mL after 3 days, respectively (Iafisco et al., 2016). As regards drug loading concentrations, in literature there are heterogeneous data about MTX, which range from 0.1 to 100 μ M (Sramek et al., 2016) to >100 μ M in case of primary SAOS cell line (Sramek et al., 2016). About DOX, the tested concentration range is 10–320 μ M for several 3D culture, including OS cell line (U2-OS) (Baek et al., 2016). In this study, we show that both SrCPC-MTX and SrCPC-DOX scaffolds exert an *in vitro* antiproliferative activity against cancer cells. Indeed, a decreasing number of SAOS-eGFP cells were observed at Day 7 in MTX/DOX-conjugated scaffolds compared to drug-free SrCPC. These data were supported by quantitative results obtained by fluorescence analysis of engineered SAOS-eGFP cells. Indeed, images from confocal microscopy analysis and measurement of fluorescence intensity revealed a reduced number of cancer cells grown on SrCPC-MTX compared to the control (52%) and a higher decrease of SAOS-eGFP cells grown on SrCPC-DOX scaffold (28%).

Similarly, SEM investigation allowed to analyse the morphology of cells grown on scaffolds. Microscopic analyses verified that the drug-free SrCPC scaffold surface was completely covered with SAOS cells, with unaltered morphology. Contrariwise, SAOS cells in contact with SrCPC-MTX presented an altered morphology. Furthermore, only a few SAOS cells were observed on the SrCPC-DOX scaffold. The doped materials observed under SEM appear to induce the loss of external projections of the U2-OS, reducing cell–cell contacts.

SrCPC-DOX induced apoptosis of SAOS-2 and U2-OS after 4 days of culture. Overall, these results report on the cytotoxic effects of MTX and DOX drug in the used concentrations. On the other hand, it is evident that 5 μ g/mL of DOX displayed a cell-killing effect on OS cell lines higher than 45 μ g/mL of MTX. This suggests that MTX concentration used herein is not sufficient to kill all SAOS cells. Contrariwise, DOX concentration could be reduced (Zhou et al., 2017).

Apoptosis is a form of programmed cell death that initiated by a tightly regulated signalling cascade, which results in caspase activation. To test the potential to induce apoptosis in SAOS-2 and U2-OS cell lines grown on doped materials, three different methods were employed. Our results indicate that SrCPC-DOX and SrCPC-MTX materials induce the apoptotic process in OS cells through the activation of the protein caspase 3/7, compared to the control material. In addition, SrCPC-DOX induces a higher expression of caspase-3 quantified with ELISA assay in SAOS-2 and U2-OS lines compared to cells grown on SrCPC-MTX and on the control material. In addition, annexin-positive test reveals that SrCPC-MTX induces an important apoptotic effect in both OS cells, while a necrotic effect was detected in OS cell lines grown on SrCPC-DOX material.

Further *in vitro* investigations are needed to deepen the genetic and epigenetic influences of drug-delivery scaffolds.

The SrCPC scaffold was tested in terms of cytocompatibility and osteoinductivity using hASCs. The SrCPC scaffolds were selected for controlled drug delivery, as they exhibit a chemically active surface, especially for apatitic phases, favouring the chemical binding of drugs (Sarda et al., 2018), as well as a microporous structure, given by nanosized acicular apatitic grains physically interlaced to form a mechanically resistant construct. Viability analyses for metabolic activity and cell morphology on drug-loaded SrCPCs report on an increasing number of live cells, as well as on the control. In addition, hASCs grown in contact with the SrCPC scaffold exhibit a well-organized cytoskeleton architecture with actin filaments being distributed uniformly in cell cytoplasm, at Day 14. In addition, the SrCPCs studied herein present a granular structure offering a good microenvironment for adhesion and proliferation of hASCs, as shown by SEM analysis where cells grew well on the scaffold surface. Cellular biology results were supported by molecular genetic/biology data, such as gene expression analysis carried out using a PCR array technique to evaluate the ECM and cell adhesion molecules profile. In bone, the ECM regulates cell adhesion, proliferation and differentiation, producing collagen, integrin, fibronectin and connective tissue growth factor (Ren et al., 2011). Moreover, osteogenic differentiation during the ECM secretion phase in MSCs induces morphological changes in immature osteoblasts, immediately followed by the formation of mature osteoblasts (Paiva & Granjeiro, 2017). In hASCs, genes encoding cell adhesion molecules were upregulated in the presence of SrCPC scaffold, demonstrating the ability of the scaffold to mediate cell–cell and/or cell–scaffold interactions. Among them, ICAM1, PECAM1, VCAM1, SELL and CD44 molecule upregulation was observed. SELL is a calcium-dependent lectin that mediates cell adhesion by binding to glycoproteins on neighbouring cells (Wedepohl et al., 2017), whereas CD44 molecule is responsible for cell–cell interactions engaging ECM components, such as hyaluronan, collagen, growth factors, cytokines or proteases (Midgley et al., 2013). ECM–cell interaction is crucial for tissue morphogenesis and architecture, thus such actions are mediated by integrin and cadherin (Di Benedetto et al., 2015). The SrCPC scaffold stimulated the upregulation of genes encoding integrins and cadherins in hASCs. Early expressed integrins are ITGA2 and ITGB3 followed by

ITGA3/4/6/8, which were upregulated up to Day 14. The gene expression levels of *ITGA2* and *ITGA3* were in agreement in the two different PCR-Array for ECM and Osteogenesis, as well as *ITGA1*, which resulted downregulated in both assays, at the first time point. Of all, the cadherin *CDH1*, a calcium-dependent cell adhesion protein, resulted upregulated in hASCs grown on the biomaterial. Integrins and cadherins have an important role in proper development, function, regeneration of skeletal tissue and MSCs osteogenic differentiation (Di Benedetto et al., 2015; Docheva et al., 2014). Collagen is the most abundant constituent of the ECM acting as a mechanical support for cells (Saito & Marumo, 2015). In vitro results demonstrated that the SrCPC scaffold promoted the expression of genes encoding for collagen proteins including *COL7/8/11/14/15A1*. The latter is constantly up-expressed during the experimental time course in both the PCRs assay thus highlighting its important role in osteogenic differentiation and mineralization (Wu et al., 2020). MMPs, with the ability to cleave collagens and proteoglycans, are among the most active proteases in ECM regulation (Paiva & Granjeiro, 2017). Such proteinases are involved in wound healing and tissue remodelling (Milner & Cawston, 2005). *MMP1/3/11* gene expression was promptly induced by SrCPC in hASCs. *MMP8/15* were positively modulated by the scaffold later. Indeed, while *MMP15* is a membrane-type metalloproteinase (Liang et al., 2016), *MMP8* is expressed in osteoblastic progenitors, differentiated osteoblasts and osteocytes (Sasano et al., 2002). Moreover, *MMP10*, which is essential for human bone development (Bord et al., 1998) and takes part in the physiological processes of bone growth (Ortega et al., 2004), resulted positively modulated by the SrCPC scaffold. The *BMP2* gene resulted upregulated in our experiments, suggesting hASCs osteogenic differentiation upon contact with the scaffold. Further, it has been reported that *MMP10* enhances BMP-2-induced osteoblast differentiation in vitro (Reyes et al., 2018). The crucial signalling pathways leading MSCs towards osteogenesis differentiation are *TGF- β* and *BMP* (Lanzillotti et al., 2021; Mazziotta et al., 2021). Our results demonstrate that SrCPC scaffold upregulated genes are involved in these two signalling cascades. Specifically, three of the most important BMPs, involved in osteogenesis, that is, *BMP2/4/7*, resulted upregulated alongside other BMP signalling like *BMPR1A*, *BMPR2* and *SMAD5* (Martini et al., 2020). On the other hand, among factors involved in the *TGF- β* cascade, *TGFBR1/2* were positively regulated by the scaffold. The activation of cited signalling pathways leads to the expression of master osteogenic transcription factors, such as *RUNX2* and *OSX*, also known as *SP7*. More precisely, *OSX* is a downstream *RUNX2* gene (laquinta et al., 2021a). Our results are in agreement with previous reports in as much as they demonstrated that the *RUNX2* gene was upregulated at Days 3 and 6, whereas *SP7* expression with high FC is observed at Day 14, when *RUNX2* modulation disappears (laquinta et al., 2021a). Finally, *RUNX2* and *SP7* activity results in specific osteoblast gene expression of including *OCN* and collagen (laquinta et al., 2021a). SrCPC biomaterial induced *OCN* upregulation in term of gene (*BGLAP*) and protein (*OCN*) expressions. In agreement, matrix

mineralization analysis showed an increase matrix deposition in hASCs grown on the scaffold, as well as the upregulation of *ALPL* gene. Other osteogenic genes involved in the skeletal development process were modulated in hASCs by the scaffold. Of these, upregulation of *GLI1* and *EGFR* was observed. *GLI1* is a transcriptional activator involved in signalling-mediated specification for osteoblast lineage inducing early osteoblast differentiation (Hojo et al., 2012). On the other hand, *EGFR* take part in *EGFR/ERK/IGFBP-3* signalling pathway inducing osteoblast differentiation and maturation (Mazzoni et al., 2020). Additionally, the *CLEC3B* gene was found to be expressed in hASCs grown on the biomaterial, up to Day 14 (Larsen et al., 2010).

It is well known that when MSCs differentiate into osteoblasts many osteoclast-associated cytokines are secreted, including *CSF*, *RANKL*-stimulating osteoclasts differentiation (Meng et al., 2020). Our experiments revealed the upregulation of *TNFSF11*, also known as *RANKL*, and *CSF2/3* genes. Thus, in hASCs the mechanism of bone resorption is activated together with the bone formation process. The coupled mechanisms continuously lead to bone remodelling. Our data show an antiproliferative ability of nanostructured apatitic bone cements (SrCPC) loaded with drugs on OS cells, with a greater effect of the SrCPC-DOX scaffold compared to SrCPC-MTX. The SrCPC scaffold, free of any loaded drugs, exhibits cytocompatibility and inductive effects on hASC osteogenic differentiation. However, further studies should be carry out to evaluate if SrCPC-DOX and SrCPC-MTX may affect different hASC biological processes depending on drug concentration. These combined effects are promising for new therapeutic strategies against OS, addressing both tumour eradication and bone regeneration. A critical point is related to the setup of appropriate dosage of anticancer drugs with time, which has to be tuned to balance toxic effects given by the drugs and the positive osteogenic signalling provided by the scaffold, as induced by their inherent physico-chemical and structural features. In this respect, nanostructured apatitic scaffolds, such as SrCPC, are particularly promising as the chemically active surface and the diffuse microporosity typical of self-hardened apatitic cements permit chemical linking of a variety of drugs and their incorporation into hollow cavities from which drugs can be released by diffusive mechanisms. Such results provide interesting observations about the innovative materials doped with chemioterapeutic drugs (metatrexate and DOX) that deserve to be studied in an animal model or 3D organoids. Reliable animal models that can accurately recapitulate the disease are required. At present, no information is available in literature about the use of SrCPC as a carrier of anticancer agents including MTX and DOX. Hence, our study aims to assess the effectiveness, in vivo, of localized drug treatments through an implantable scaffold, thus targeting new therapies for patients with OS, promising to limit the risks of relapse, metastasis and systemic toxicity related to the use of systemic chemotherapy. In addition, the study also aims to search for new deregulated biological molecules that support chemoresistance and that can bio-functionalize the bioactive scaffolds to be used in OS patients.

AUTHOR CONTRIBUTIONS

Carmen Lanzillotti and Maria Rosa Iaquina: Investigation, formal analysis, writing. **Raffaella De Pace, Maria Mosaico, Simone Patergnani:** Methodology, formal analysis, data curation. **Carlotta Giorgi, Simone Sprio, Massimiliano Dapporto, Marta Tavoni, Anna Tampieri:** Investigation, visualization. **Elisa Mazzoni, Monica Montesi, Martini Fernanda:** Grant acquisition, validation, supervision and writing.

ACKNOWLEDGEMENTS

Dr. Paola Boldrini's technical assistance is gratefully acknowledged for the SEM analysis performed at the Center of Electron Microscopy, University of Ferrara, Ferrara, Italy. The authors thank Professor Georgia Emma Gili for revising the English text of the manuscript. The PhD student Carmen Lanzillotti was a fellowship recipient of the Emilia Romagna Region with the fund dedicated to the High Education in Research, which was supported by the grant POR FSE, European Union. This study was supported, in part, by grant from (i) Ministero della Università e della Ricerca (MUR) PRIN 2017, project code C8RYSS to Fernanda Martini and Monica Montesi, (ii) University of Ferrara, Fondo di Ateneo per la Ricerca, grants FAR 2021 to Elisa Mazzoni and Fernanda Martini.

CONFLICT OF INTEREST STATEMENT

The authors declare no conflict of interest.

ORCID

Monica Montesi  <http://orcid.org/0000-0002-9192-8554>

Fernanda Martini  <http://orcid.org/0000-0001-9137-0805>

Elisa Mazzoni  <http://orcid.org/0000-0001-6829-8569>

REFERENCES

- Ahmed, L., Atif, R., Eldeen, T. S., Yahya, I., Omara, A., & Eltayeb, M. (2019). Study the using of nanoparticles as drug delivery system based on mathematical models for controlled release. *International Journal of Latest Technology in Engineering, Management & Applied Science*, 8, 52–56.
- Baek, N., Seo, O. W., Kim, M., Hulme, J., & An, S. S. A. (2016). Monitoring the effects of doxorubicin on 3D-spheroid tumor cells in real-time. *OncoTargets and Therapy*, 9, 7207–7218. <https://doi.org/10.2147/OTT.S112566>
- Beaury, M. W., Kelly-Beaury, M. L., Sharp, G., & Cottrell, J. A. (2018). Review of Osteosarcoma therapeutics. *Journal of Cancer Treatment and Diagnosis*. <https://doi.org/10.29245/2578-2967/2018/2.1127>
- Belayneh, R., Fourman, M. S., Bhogal, S., & Weiss, K. R. (2021). Update on osteosarcoma. *Current Oncology Reports*, 23(6), 71. <https://doi.org/10.1007/s11912-021-01053-7>
- Di Benedetto, A., Brunetti, G., Posa, F., Ballini, A., Grassi, F. R., Colaianni, G., Colucci, S., Rossi, E., Cavalcanti-Adam, E. A., Lo Muzio, L., Grano, M., & Mori, G. (2015). Osteogenic differentiation of mesenchymal stem cells from dental bud: Role of integrins and cadherins. *Stem Cell Research*, 15(3), 618–628. <https://doi.org/10.1016/j.scr.2015.09.011>
- Bischoff, I., Tsaryk, R., Chai, F., Fürst, R., Kirkpatrick, C. J., & Unger, R. E. (2018). In vitro evaluation of a biomaterial-based anticancer drug delivery system as an alternative to conventional post-surgery bone cancer treatment. *Materials Science & Engineering, C: Materials for Biological Applications*, 93, 115–124. <https://doi.org/10.1016/j.msec.2018.07.057>
- Bishop, M. W., Janeway, K. A., & Gorlick, R. (2016). Future directions in the treatment of osteosarcoma. *Current Opinion in Pediatrics*, 28(1), 26–33. <https://doi.org/10.1097/MOP.0000000000000298>
- Bord, S., Horner, A., Hembry, R. M., & Compston, J. E. (1998). Stromelysin-1 (MMP-3) and stromelysin-2 (MMP-10) expression in developing human bone: Potential roles in skeletal development. *Bone*, 23(1), 7–12. [https://doi.org/10.1016/S8756-3282\(98\)00064-7](https://doi.org/10.1016/S8756-3282(98)00064-7)
- Bruschi, M. L. (Ed.). (2015). 5—Mathematical models of drug release, *Strategies to modify the drug release from pharmaceutical systems* (pp. 63–86). Woodhead Publishing. <https://doi.org/10.1016/B978-0-08-100092-2.00005-9>
- Chen, J., Chen, X., Chen, X., Sun, H., & Yang, D. (2019). SM-164 enhances the antitumor activity of adriamycin in human U2-OS cells via downregulation of X-linked inhibitor of apoptosis protein. *Molecular Medicine Reports*, 19(6), 5079–5086. <https://doi.org/10.3892/mmr.2019.10181>
- Corre, I., Verrecchia, F., Crenn, V., Redini, F., & Trichet, V. (2020). The osteosarcoma microenvironment: A complex but targetable ecosystem. *Cells*, 9(4), 976. <https://doi.org/10.3390/cells9040976>
- Cui, X., Zhang, Y., Wang, J., Huang, C., Wang, Y., Yang, H., Liu, W., Wang, T., Wang, D., Wang, G., Ruan, C., Chen, D., Lu, W. W., Huang, W., Rahaman, M. N., & Pan, H. (2020). Strontium modulates osteogenic activity of bone cement composed of bioactive borosilicate glass particles by activating Wnt/ β -catenin signaling pathway. *Bioactive Materials*, 5(2), 334–347. <https://doi.org/10.1016/j.bioactmat.2020.02.016>
- Dapporto, M., Gardini, D., Tampieri, A., & Sprio, S. (2021). Nanostructured strontium-doped calcium phosphate cements: A multifactorial design. *Applied Sciences*, 11(5), 2075. <https://doi.org/10.3390/app11052075>
- Docheva, D., Popov, C., Alberton, P., & Aszodi, A. (2014). Integrin signaling in skeletal development and function. *Birth Defects Research Part C: Embryo Today: Reviews*, 102(1), 13–36. <https://doi.org/10.1002/bdrc.21059>
- Fosca, M., Rau, J. V., & Uskoković, V. (2022). Factors influencing the drug release from calcium phosphate cements. *Bioactive Materials*, 7, 341–363. <https://doi.org/10.1016/j.bioactmat.2021.05.032>
- Gaebler, M., Silvestri, A., Haybaeck, J., Reichardt, P., Lowery, C. D., Stancato, L. F., Zybarth, G., & Regenbrecht, C. R. A. (2017). Three-dimensional patient-derived in vitro sarcoma models: promising tools for improving clinical tumor management. *Frontiers in Oncology*, 7, 203. <https://doi.org/10.3389/fonc.2017.00203>
- Giorgi, C., Bonora, M., Missiroli, S., Poletti, F., Ramirez, F. G., Morciano, G., Morganti, C., Pandolfi, P. P., Mammanno, F., & Pinton, P. (2014). Intravital imaging reveals p53-dependent cancer cell death induced by phototherapy via calcium signaling. *Oncotarget*, 6(3), 1435–1445.
- Globig, P., Willumeit-Römer, R., Martini, F., Mazzoni, E., & Luthringer-Feyerabend, B. J. C. (2020). Optimizing an osteosarcoma-fibroblast coculture model to study antitumoral activity of magnesium-based biomaterials. *International Journal of Molecular Sciences*, 21(14), 5099. <https://doi.org/10.3390/ijms21145099>
- Harrison, D. J., & Schwartz, C. L. (2017). Osteogenic sarcoma: systemic chemotherapy options for localized disease. *Current Treatment Options in Oncology*, 18(4), 24. <https://doi.org/10.1007/s11864-017-0464-2>
- Hojo, H., Ohba, S., Yano, F., Saito, T., Ikeda, T., Nakajima, K., Komiyama, Y., Nakagata, N., Suzuki, K., Takato, T., Kawaguchi, H., & Chung, U. (2012). Gli1 protein participates in Hedgehog-mediated specification of osteoblast lineage during endochondral ossification. *Journal of Biological Chemistry*, 287(21), 17860–17869. <https://doi.org/10.1074/jbc.M112.347716>
- Ho-Shui-Ling, A., Bolander, J., Rustom, L. E., Johnson, A. W., Luyten, F. P., & Picart, C. (2018). Bone regeneration strategies: Engineered

- scaffolds, bioactive molecules and stem cells current stage and future perspectives. *Biomaterials*, 180, 143–162. <https://doi.org/10.1016/j.biomaterials.2018.07.017>
- Iafisco, M., Drouet, C., Adamiano, A., Pascaud, P., Montesi, M., Panseri, S., Sarda, S., & Tampieri, A. (2016). Superparamagnetic iron-doped nanocrystalline apatite as a delivery system for doxorubicin. *Journal of Materials Chemistry, B*, 4(1), 57–70. <https://doi.org/10.1039/c5tb01524c>
- Iaquinta, M. R., Lanzillotti, C., Mazziotta, C., Bononi, I., Frontini, F., Mazzoni, E., Oton-Gonzalez, L., Rotondo, J. C., Torreggiani, E., Tognon, M., & Martini, F. (2021a). The role of microRNAs in the osteogenic and chondrogenic differentiation of mesenchymal stem cells and bone pathologies. *Theranostics*, 11, 6573–6591.
- Iaquinta, M. R., Martini, F., D'Agostino, A., Trevisiol, L., Bersani, M., Torreggiani, E., Tognon, M., Rotondo, J. C., & Mazzoni, E. (2022). Stem cell fate and immunomodulation promote bone regeneration via composite Bio-Oss®/AviteneTM biomaterial. *Frontiers in Bioengineering and Biotechnology*, 10, 873814. <https://doi.org/10.3389/fbioe.2022.873814>
- Iaquinta, M. R., Mazzoni, E., Bononi, I., Rotondo, J. C., Mazziotta, C., Montesi, M., Sprio, S., Tampieri, A., Tognon, M., & Martini, F. (2019). Adult stem cells for bone regeneration and repair. *Frontiers in Cell and Developmental Biology*, 7, 268. <https://doi.org/10.3389/fcell.2019.00268>
- Iaquinta, M. R., Torreggiani, E., Mazziotta, C., Ruffini, A., Sprio, S., Tampieri, A., Tognon, M., Martini, F., & Mazzoni, E. (2021b). In vitro osteoinductivity assay of hydroxylapatite scaffolds, obtained with biomorphic transformation processes, assessed using human adipose stem cell cultures. *International Journal of Molecular Sciences*, 22(13), 7092. <https://doi.org/10.3390/ijms22137092>
- Jackson, T. M., Bittman, M., & Granowetter, L. (2016). Pediatric malignant bone tumors: A review and update on current challenges, and emerging drug targets. *Current Problems in Pediatric and Adolescent Health Care*, 46(7), 213–228. <https://doi.org/10.1016/j.cppeds.2016.04.002>
- Jafari, F., Javdansirat, S., Sanaie, S., Naseri, A., Shamekh, A., Rostamzadeh, D., & Dolati, S. (2020). Osteosarcoma: A comprehensive review of management and treatment strategies. *Annals of Diagnostic Pathology*, 49, 151654. <https://doi.org/10.1016/j.anndiagpath.2020.151654>
- Janeway, K. A., & Grier, H. E. (2010). Sequelae of osteosarcoma medical therapy: A review of rare acute toxicities and late effects. *The Lancet Oncology*, 11(7), 670–678. [https://doi.org/10.1016/S1470-2045\(10\)70062-0](https://doi.org/10.1016/S1470-2045(10)70062-0)
- Korsmeyer, R. W., Gurny, R., Doelker, E., Buri, P., & Peppas, N. A. (1983). Mechanisms of solute release from porous hydrophilic polymers. *International Journal of Pharmaceutics*, 15(1), 25–35. [https://doi.org/10.1016/0378-5173\(83\)90064-9](https://doi.org/10.1016/0378-5173(83)90064-9)
- Kumar, R., Kumar, M., Malhotra, K., & Patel, S. (2018). Primary osteosarcoma in the elderly revisited: current concepts in diagnosis and treatment. *Current Oncology Reports*, 20(2), 13. <https://doi.org/10.1007/s11912-018-0658-1>
- Lanzillotti, C., De Mattei, M., Mazziotta, C., Taraballi, F., Rotondo, J. C., Tognon, M., & Martini, F. (2021). Long non-coding RNAs and microRNAs interplay in osteogenic differentiation of mesenchymal stem cells. *Frontiers in Cell and Developmental Biology*, 9, 646032. <https://doi.org/10.3389/fcell.2021.646032>
- Larsen, K. H., Frederiksen, C. M., Burns, J. S., Abdallah, B. M., & Kassem, M. (2010). Identifying a molecular phenotype for bone marrow stromal cells with in vivo bone-forming capacity. *Journal of Bone and Mineral Research*, 25(4), 796–808. <https://doi.org/10.1359/jbmr.091018>
- Lewis, V. O. (2005). Limb salvage in the skeletally immature patient. *Current Oncology Reports*, 7(4), 285–292. <https://doi.org/10.1007/s11912-005-0052-7>
- Liang, H. P. H., Xu, J., Xue, M., & Jackson, C. (2016). Matrix metalloproteinases in bone development and pathology: Current knowledge and potential clinical utility. *Metalloproteinases in Medicine*, 3, 93–102. <https://doi.org/10.2147/MNM.S92187>
- Liao, J., Han, R., Wu, Y., & Qian, Z. (2021). Review of a new bone tumor therapy strategy based on bifunctional biomaterials. *Bone Research*, 9(1), 18. <https://doi.org/10.1038/s41413-021-00139-z>
- Liu, Q., Liu, C., Wang, W., Yuan, L., Wang, Y., Yi, X., Pan, Z., & Yu, A. (2023). Bioinspired strontium magnesium phosphate cement prepared utilizing the precursor method for bone tissue engineering. *Frontiers in Bioengineering and Biotechnology*, 11, 1142095. <https://doi.org/10.3389/fbioe.2023.1142095>
- Manfrini, M., Di Bona, C., Canella, A., Lucarelli, E., Pellati, A., D'Agostino, A., Barbanti-Brodano, G., & Tognon, M. (2013). Mesenchymal stem cells from patients to assay bone graft substitutes. *Journal of Cellular Physiology*, 228(6), 1229–1237. <https://doi.org/10.1002/jcp.24276>
- Manfrini, M., Mazzoni, E., Barbanti-Brodano, G., Nocini, P., D'agostino, A., Trombelli, L., & Tognon, M. (2015). Osteoconductivity of complex biomaterials assayed by fluorescent-engineered osteoblast-like cells. *Cell Biochemistry and Biophysics*, 71(3), 1509–1515. <https://doi.org/10.1007/s12013-014-0374-x>
- Marie, P. (2005). Strontium as therapy for osteoporosis. *Current Opinion in Pharmacology*, 5(6), 633–636. <https://doi.org/10.1016/j.coph.2005.05.005>
- Martini, F., Pellati, A., Mazzoni, E., Salati, S., Caruso, G., Contartese, D., & De Mattei, M. (2020). Bone morphogenetic protein-2 signaling in the osteogenic differentiation of human bone marrow mesenchymal stem cells induced by pulsed electromagnetic fields. *International Journal of Molecular Sciences*, 21(6), 2104. <https://doi.org/10.3390/ijms21062104>
- Mazziotta, C., Lanzillotti, C., Iaquinta, M. R., Taraballi, F., Torreggiani, E., Rotondo, J. C., Otòn-Gonzalez, L., Mazzoni, E., Frontini, F., Bononi, I., De Mattei, M., Tognon, M., & Martini, F. (2021). MicroRNAs modulate signaling pathways in osteogenic differentiation of mesenchymal stem cells. *International Journal of Molecular Sciences*, 22(5), 2362. <https://doi.org/10.3390/ijms22052362>
- Mazzoni, E., D'Agostino, A., Iaquinta, M. R., Bononi, I., Trevisiol, L., Rotondo, J. C., Patergnani, S., Giorgi, C., Gunson, M. J., Arnett, G. W., Nocini, P. F., Tognon, M., & Martini, F. (2020). Hydroxylapatite-collagen hybrid scaffold induces human adipose-derived mesenchymal stem cells to osteogenic differentiation in vitro and bone regrowth in patients. *Stem Cells Translational Medicine*, 9(3), 377–388. <https://doi.org/10.1002/sctm.19-0170>
- Mazzoni, E., D'Agostino, A., Manfrini, M., Maniero, S., Puozzo, A., Bassi, E., Marsico, S., Fortini, C., Trevisiol, L., Patergnani, S., & Tognon, M. (2017). Human adipose stem cells induced to osteogenic differentiation by an innovative collagen/hydroxylapatite hybrid scaffold. *The FASEB Journal*, 31(10), 4555–4565. <https://doi.org/10.1096/fj.201601384R>
- Mazzoni, E., Iaquinta, M. R., Lanzillotti, C., Mazziotta, C., Maritati, M., Montesi, M., Sprio, S., Tampieri, A., Tognon, M., & Martini, F. (2021a). Bioactive materials for soft tissue repair. *Frontiers in Bioengineering and Biotechnology*, 9, 613787. <https://doi.org/10.3389/fbioe.2021.613787>
- Mazzoni, E., Iaquinta, M. R., Mosaico, M., De Pace, R., D'Agostino, A., Tognon, M., & Martini, F. (2023). Human mesenchymal stem cells and innovative scaffolds for bone tissue engineering applications. *Tissue Engineering Part B: Reviews*, 29(5), 514–531. <https://doi.org/10.1089/ten.teb.2022.0217>
- Mazzoni, E., Mazziotta, C., Iaquinta, M. R., Lanzillotti, C., Fortini, F., D'Agostino, A., Trevisiol, L., Nocini, R., Barbanti-Brodano, G., Mescola, A., Alessandrini, A., Tognon, M., & Martini, F. (2021b). Enhanced osteogenic differentiation of human bone marrow-derived mesenchymal stem cells by a hybrid hydroxylapatite/

- collagen scaffold. *Frontiers in Cell and Developmental Biology*, 8, 610570. <https://doi.org/10.3389/fcell.2020.610570>
- Meng, B., Wu, D., Cheng, Y., Huang, P., Liu, Y., Gan, L., Liu, C., & Cao, Y. (2020). Interleukin-20 differentially regulates bone mesenchymal stem cell activities in RANKL-induced osteoclastogenesis through the OPG/RANKL/RANK axis and the NF- κ B, MAPK and AKT signalling pathways. *Scandinavian Journal of Immunology*, 91(5), e12874. <https://doi.org/10.1111/sji.12874>
- Midgley, A. C., Rogers, M., Hallett, M. B., Clayton, A., Bowen, T., Phillips, A. O., & Steadman, R. (2013). Transforming growth factor- β 1 (TGF- β 1)-stimulated fibroblast to myofibroblast differentiation is mediated by hyaluronan (HA)-facilitated epidermal growth factor receptor (EGFR) and CD44 co-localization in lipid rafts. *Journal of Biological Chemistry*, 288(21), 14824–14838. <https://doi.org/10.1074/jbc.M113.451336>
- Milner, J., & Cawston, T. (2005). Matrix metalloproteinase knockout studies and the potential use of matrix metalloproteinase inhibitors in the rheumatic diseases. *Current Drug Target Inflammation & Allergy*, 4(3), 363–375. <https://doi.org/10.2174/1568010054022141>
- Mirabello, L., Troisi, R. J., & Savage, S. A. (2009). International osteosarcoma incidence patterns in children and adolescents, middle ages and elderly persons. *International Journal of Cancer*, 125(1), 229–234. <https://doi.org/10.1002/ijc.24320>
- Montesi, M., Panseri, S., Dapporto, M., Tampieri, A., & Sprio, S. (2017). Sr-substituted bone cements direct mesenchymal stem cells, osteoblasts and osteoclasts fate. *PLoS One*, 12(2), e0172100. <https://doi.org/10.1371/journal.pone.0172100>
- Morelli, C., Barbanti-Brodano, G., Ciannilli, A., Campioni, K., Boriani, S., & Tognon, M. (2007). Cell morphology, markers, spreading, and proliferation on orthopaedic biomaterials. An innovative cellular model for the 'in vitro' study. *Journal of biomedical materials research. Part A*, 83(1), 178–183. <https://doi.org/10.1002/jbm.a.31262>
- Mukesh, U., Kulkarni, V., Tushar, R., & Murthy, R. S. R. (2009). Methotrexate loaded self stabilized calcium phosphate nanoparticles: A novel inorganic carrier for intracellular drug delivery. *Journal of Biomedical Nanotechnology*, 5(1), 99–105. <https://doi.org/10.1166/jbn.2009.026>
- Mutsaers, A. J., & Walkley, C. R. (2014). Cells of origin in osteosarcoma: Mesenchymal stem cells or osteoblast committed cells? *Bone*, 62, 56–63. <https://doi.org/10.1016/j.bone.2014.02.003>
- Ortega, N., Behonick, D. J., & Werb, Z. (2004). Matrix remodeling during endochondral ossification. *Trends in Cell Biology*, 14(2), 86–93. <https://doi.org/10.1016/j.tcb.2003.12.003>
- Oton-Gonzalez, L., Mazziotta, C., Iaquina, M. R., Mazzoni, E., Nocini, R., Trevisiol, L., D'Agostino, A., Tognon, M., Rotondo, J. C., & Martini, F. (2022). Genetics and epigenetics of bone remodeling and metabolic bone diseases. *International Journal of Molecular Sciences*, 23(3), 1500. <https://doi.org/10.3390/ijms23031500>
- Ottaviani, G., & Jaffe, N. (2009). The epidemiology of osteosarcoma. *Cancer Treatment and Research*, 152, 3–13. https://doi.org/10.1007/978-1-4419-0284-9_1
- Paarakh, M. P., Jose, P. A. N. I., Setty, C. M., & Peter, G. V. (2019). Release kinetics – Concepts and applications. *International Journal of Pharmacy Research & Technology*, 8(1), 12–20. <https://doi.org/10.31838/ijprt/08.01.02>
- Paiva, K. B. S., & Granjeiro, J. M. (2017). Matrix metalloproteinases in bone resorption, remodeling, and repair. *Progress in Molecular Biology and Translational Science*, 148, 203–303. <https://doi.org/10.1016/bs.pmbts.2017.05.001>
- Pylostomou, A., Demir, Ö., & Loca, D. (2023). Calcium phosphate bone cements as local drug delivery systems for bone cancer treatment. *Biomaterials Advances*, 148, 213367. <https://doi.org/10.1016/j.bioadv.2023.213367>
- Ren, J., Jin, P., Sabatino, M., Balakumaran, A., Feng, J., Kuznetsov, S. A., Klein, H. G., Robey, P. G., & Stroncek, D. F. (2011). Global transcriptome analysis of human bone marrow stromal cells (BMSC) reveals proliferative, mobile and interactive cells that produce abundant extracellular matrix proteins, some of which may affect BMSC potency. *Cytotherapy*, 13(6), 661–674. <https://doi.org/10.3109/14653249.2010.548379>
- Reyes, R., Rodríguez, J. A., Orbe, J., Arnau, M. R., Évora, C., & Delgado, A. (2018). Combined sustained release of BMP2 and MMP10 accelerates bone formation and mineralization of calvaria critical size defect in mice. *Drug Delivery*, 25(1), 750–756. <https://doi.org/10.1080/10717544.2018.1446473>
- Ritter, J., & Bielack, S. S. (2010). Osteosarcoma. *Annals of Oncology*, 21(Suppl. 7), vii320–vii325. <https://doi.org/10.1093/annonc/mdq276>
- Saito, M., & Marumo, K. (2015). Effects of collagen crosslinking on bone material properties in health and disease. *Calcified Tissue International*, 97(3), 242–261. <https://doi.org/10.1007/s00223-015-9985-5>
- Sarda, S., Iafisco, M., Pascaud-Mathieu, P., Adamiano, A., Montesi, M., Panseri, S., Marsan, O., Thouron, C., Dupret-Bories, A., Tampieri, A., & Drouet, C. (2018). Interaction of folic acid with nanocrystalline apatites and extension to methotrexate (Antifolate) in view of anticancer applications. *Langmuir*, 34(40), 12036–12048. <https://doi.org/10.1021/acs.langmuir.8b02602>
- Sasano, Y., Zhu, J.-X., Tsubota, M., Takahashi, I., Onodera, K., Mizoguchi, I., & Kagayama, M. (2002). Gene expression of MMP8 and MMP13 during embryonic development of bone and cartilage in the rat mandible and hind limb. *Journal of Histochemistry & Cytochemistry*, 50(3), 325–332. <https://doi.org/10.1177/002215540205000304>
- Schumacher, M., & Gelinsky, M. (2015). Strontium modified calcium phosphate cements – Approaches towards targeted stimulation of bone turnover. *Journal of Materials Chemistry B*, 3(23), 4626–4640. <https://doi.org/10.1039/C5TB00654F>
- Sobczak, M., & Kędra, K. (2022). Biomedical polyurethanes for Anti-Cancer drug delivery systems: A brief, comprehensive review. *International Journal of Molecular Sciences*, 23(15), 8181. <https://doi.org/10.3390/ijms23158181>
- Son, K. D., & Kim, Y.-J. (2017). Anticancer activity of drug-loaded calcium phosphate nanocomposites against human osteosarcoma. *Biomaterials Research*, 21(1), 13. <https://doi.org/10.1186/s40824-017-0099-1>
- Sprio, S., Dapporto, M., Montesi, M., Panseri, S., Lattanzi, W., Pola, E., Logroscino, G., & Tampieri, A. (2016). Novel osteointegrative Sr-substituted apatitic cements enriched with alginate. *Materials*, 9(9), 763. <https://doi.org/10.3390/ma9090763>
- Sprio, S., Dapporto, M., Preti, L., Mazzoni, E., Iaquina, M. R., Martini, F., Tognon, M., Pugno, N. M., Restivo, E., Visai, L., & Tampieri, A. (2020). Enhancement of the biological and mechanical performances of sintered hydroxyapatite by multiple ions doping. *Frontiers in Materials*, 7, 224. <https://doi.org/10.3389/fmats.2020.00224>
- Sramek, M., Neradil, J., Sterba, J., & Veselska, R. (2016). Non-DHFR-mediated effects of methotrexate in osteosarcoma cell lines: Epigenetic alterations and enhanced cell differentiation. *Cancer Cell International*, 16, 14. <https://doi.org/10.1186/s12935-016-0289-2>
- Suksiriworapong, J., Taresco, V., Ivanov, D. P., Styliari, I. D., Sakchaisri, K., Junyaprasert, V. B., & Garnett, M. C. (2018). Synthesis and properties of a biodegradable polymer-drug conjugate: Methotrexate-poly(glycerol adipate). *Colloids and Surfaces B: Biointerfaces*, 167, 115–125. <https://doi.org/10.1016/j.colsurfb.2018.03.048>
- Tanzawa, Y., Tsuchiya, H., Shirai, T., Nishida, H., Hayashi, K., Takeuchi, A., Tomita, K., & Kawahara, M. (2011). Potentiation of the antitumor effect of calcium phosphate cement containing anticancer drug and caffeine on rat osteosarcoma. *Journal of Orthopaedic Science*, 16(1), 77–84. <https://doi.org/10.1007/s00776-011-0045-3>
- Wedepohl, S., Dervedde, J., Vahedi-Faridi, A., Tauber, R., Saenger, W., & Bulut, H. (2017). Reducing macro- and microheterogeneity of

- N-glycans enables the crystal structure of the lectin and EGF-like domains of human L-selectin to be solved at 1.9 Å resolution. *ChemBioChem*, 18(13), 1338–1345. <https://doi.org/10.1002/cbic.201700220>
- Wu, J., Ren, W., Zheng, Z., Huang, Z., Liang, T., Li, F., Shi, Z., Jiang, Q., Yang, X., & Guo, L. (2020). Mmu_circ_003795 regulates osteoblast differentiation and mineralization in MC3T3-E1 and MDPC23 by targeting COL15A1. *Molecular Medicine Reports*, 22(3), 1737–1746. <https://doi.org/10.3892/mmr.2020.11264>
- Xu, M., Xu, S. F., & Yu, X. C. (2014). Clinical analysis of osteosarcoma patients treated with high-dose methotrexate-free neoadjuvant chemotherapy. *Current Oncology*, 21(5), 678–684. <https://doi.org/10.3747/co.21.1973>
- Zhou, Z.-F., Sun, T.-W., Chen, F., Zuo, D.-Q., Wang, H.-S., Hua, Y.-Q., Cai, Z.-D., & Tan, J. (2017). Calcium phosphate-phosphorylated adenosine hybrid microspheres for anti-osteosarcoma drug delivery and osteogenic differentiation. *Biomaterials*, 121, 1–14. <https://doi.org/10.1016/j.biomaterials.2016.12.031>
- Zhu, Y., Ouyang, Y., Chang, Y., Luo, C., Xu, J., Zhang, C., & Huang, W. (2013). Evaluation of the proliferation and differentiation behaviors of mesenchymal stem cells with partially converted borate glass containing different amounts of strontium in vitro. *Molecular Medicine Reports*, 7(4), 1129–1136. <https://doi.org/10.3892/mmr.2013.1341>

SUPPORTING INFORMATION

Additional supporting information can be found online in the Supporting Information section at the end of this article.

How to cite this article: Lanzillotti, C., Iaquinta, M. R., De Pace, R., Mosaico, M., Patergnani, S., Giorgi, C., Tavoni, M., Dapporto, M., Sprio, S., Tampieri, A., Montesi, M., Martini, F., & Mazzone, E. (2024). Osteosarcoma cell death induced by innovative scaffolds doped with chemotherapeutics. *Journal of Cellular Physiology*, 239, e31256. <https://doi.org/10.1002/jcp.31256>